

# Conceptual Design of a Supersonic Air-launch System

John P. Clarke,<sup>1</sup> Kevin Cerven,<sup>1</sup> James March,<sup>1</sup> Michael Olszewski,<sup>1</sup> Brad Wheaton,<sup>1</sup> Matthew Williams,<sup>1</sup> John Yu,<sup>1</sup>  
Michael Selig,<sup>2</sup> Eric Loth,<sup>3</sup> and Rodney Burton<sup>4</sup>  
*University of Illinois, Urbana, Illinois, 61801*

**To reduce the cost of payload to orbit, a conceptual design of a supersonic air-launch system for the Space Exploration Technologies Falcon 1 rocket was performed. Several design candidates were reduced to three preliminary concepts, which in turn underwent comparative analyses to determine a final design that best fulfilled performance requirements. A 53 deg sweep, delta wing planform was chosen to balance subsonic and supersonic performance to reduce overall fuel consumption. A long nose provides balance and increased internal volume, and a canard was chosen to provide pitch control. The top-carried semi-conformal rocket payload reduces drag, while two widely spaced vertical stabilizers reduce impact risk during separation. Four F101-GE-102 afterburning turbofan engines were chosen to reduce fuel consumption. The aircraft gross take-off weight is 139,550 lb, empty weight is 54,900 lb, and maximum speed is Mach 2.45 at 50,000 ft. The Falcon 1 rocket is released at 51,800 ft at Mach 2 with an angle of inclination to the horizon of 25 deg, resulting in a  $\Delta V$  to orbit of 24,300 ft/s. The reduced  $\Delta V$  allows a reduction in propellant sufficient to double the payload to 2100 lb. A cost estimate for production of a fleet of 2-5 aircraft is performed, and predicts that the payload cost can be reduced 43% to \$3800/lb to low Earth orbit.**

---

<sup>1</sup> Student, Department of Aerospace Engineering, 306 Talbot Laboratory, MC-236, 104 South Wright Street, Urbana, Illinois 61801, and Student member, AIAA.

<sup>2</sup> Associate Professor, Department of Aerospace Engineering, 306 Talbot Laboratory, MC-236, 104 South Wright Street, Urbana, Illinois 61801, Senior Member, AIAA.

<sup>3</sup> Professor, Department of Aerospace Engineering, 306 Talbot Laboratory, MC-236, 104 South Wright Street, Urbana, Illinois 61801, Associate Fellow, AIAA.

<sup>4</sup> Professor and Interim Department Head, Department of Aerospace Engineering, 306 Talbot Laboratory, MC-236, 104 South Wright Street, Urbana, Illinois 61801, Associate Fellow, AIAA.

## I. Motivation

This design concept seeks to develop a scalable payload delivery system capable of meeting demands of a Supersonic Aircraft for Reusable Rocket Air-Launch (SARRA) of the SpaceX Falcon 1 rocket. This is an economical aircraft, shown in Fig 1, capable of a 48-hour turnaround time in launching the Falcon 1 from a minimum altitude of 50,000 ft (15,240 m) at a velocity of Mach 2.

Cost reduction of launch services was the motivation for the design of the SARRA. This motivation led to using a theme of L-3: Low Research and Development Cost, Low Manufacturing Cost and Low Operating Cost. Successful aerospace ventures, including Boeing and Southwest Airlines, have demonstrated that once performance requirements are achieved, a lower total cost is usually the primary factor in a customer's decision. This was certainly true for the Boeing C-17, when the U.S. Congress declared it would not buy more than 48 aircraft because it was too expensive. Boeing drastically reduced the costs to build the aircraft and Congress went on to buy 150 more. With this in mind, the theme of L-3 affected most decisions in the development of the SARRA.

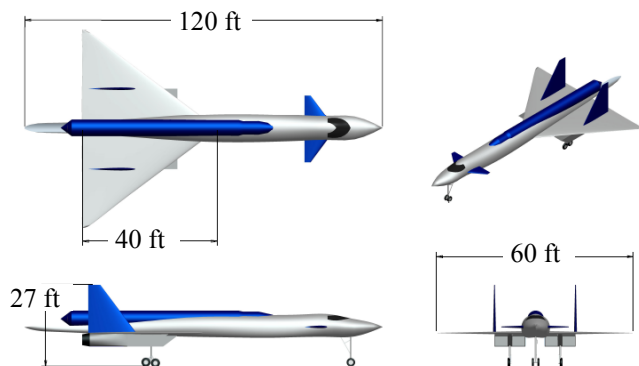


Figure 1. Three View of the SARRA

## II. Concept of Operations

The mission for the vehicle is to carry a SpaceX Falcon 1 rocket, and release it at an altitude of 50,000 ft (15,240 m) at a minimum velocity of Mach 2.0. These conditions were selected to reduce costs in payload delivery to low Earth orbit. Peak power for maximum trust is written (Burton, 2006),

$$P = \frac{1}{2} \left( \frac{T}{W_0} \right) \eta_{LEO} g^2 I_{sp} g^{2.5} \frac{\Delta V}{c} \quad (1)$$

and the launch cost (in 2004 dollars) in terms of peak power is expressed as,

$$\text{Launch Cost} = \frac{\text{Peak Power (Mega Watts)}}{100} \quad (2)$$

For the SARRA vehicle, launched at a 25 deg climb angle, the  $T/W_0$  approaches 1.0 g at Mach 2. The  $\Delta V$  to orbit is 24,278 ft/s (7,394 m/s), which results in a specific cost to orbit of \$790 per lb (\$1,740 per kg) (Burton, 2006). For the Falcon 1, the  $ISP_{vacuum}$  is 304 s and the  $ISP_{sea\ level}$  is 255 s.

The vehicle is designed with the understanding that the mission has risk for both the payload owner, aircraft owner as well as other stakeholders. With the understanding of the risks associated with launch, the vehicle has developed a number of risk mitigation techniques. The SARRA vehicle lowers the cost of operation through cost savings in a simple mission profile and a quasi-passive release mechanism. Other cost reduction considerations were taken into account in designing the concept of operation for the vehicle. Throughout the paper, material from Raymer (Raymer, 2006) was used.

**Risk Analysis.** The greatest potential for mission failure occurs with the release of the SpaceX Falcon 1 rocket from the aircraft at supersonic speeds. The first area of risk is the potential for collision between the rocket and the aircraft tails, which are vulnerable for impact. The second possible area of risk is the rocket becoming unstable and uncontrollable after release, and the third area of possible risk is drastic aerodynamic change of the aircraft after release, including a large increase in base drag.

**Risk Mitigation.** With the potential risks of the mission determined, a number of procedures and devices were developed to mitigate and eliminate the potential for failure. The method selected is a semi-conformal configuration in which the rocket is carried on top of the aircraft. To moderate the risk of collisions, the SARRA vehicle enters a parabolic flight trajectory to maneuver the aircraft and rocket into ballistic flight at the moment of release. This procedure places the rocket in a situation where the gravitational downward force is negated by the upward inertial force due to the changing rate of climb, creating a zero gravity condition where (in the aircraft and rocket frame of reference); both objects are traveling at the same velocity. The rocket will not experience horizontal loading other than aerodynamic forces while in ballistic flight. While in this condition, the rocket is mechanically accelerated on the rocket support structure toward the rear relative to the aircraft to minimize the time the rocket is within striking distance of the SARRA vehicle. The rocket support structure and aircraft move away from the rocket in order to create the largest separation between the rocket and aircraft while the rocket is in uncontrolled flight. The aircraft vertical tails are spaced far apart to prevent a tail strike, and finally, an added benefit of the top carriage method is the ability to

avoid ground debris during taxiing, taking off, and landing while reducing the size of the landing gear.

Uncontrollable oscillation and pitching of the rocket is a major concern that requires understanding to insure the payload is delivered to orbit without damage. Given the expensive nature of the payload and the limitations in modifying the rocket, an effective device to reduce oscillations while maintaining stability and orientation was developed; a conical drag device (CDD) is fitted to the rear of the Falcon 1. This CDD will deploy after the rocket is released and away from the aircraft and will control both pitch and yaw stability of the rocket for approximately 5 seconds, after which the rocket engines are able to control pitch and yaw.

The CDD used on the SARRA vehicle is shown in Fig 2. The cone is 3.66 ft (1.12 m) in length and 5.5 ft (1.68 m) in diameter. To increase further the stability of the rocket after release, the aircraft employs a top mount approach to carrying the Falcon 1. With the top carriage method, in conjunction with the ballistic flight as mentioned above, the aircraft is able to reduce the effect of bow shock on the rocket after release. The relative motion of the rocket causes the rocket to have a greater aircraft separation at the point when it may encounter adverse pitching due to the bow shocks of the aircraft.



Figure 2. Falcon 1 with Drag Cone.

The rocket carriage system incorporates a passive venting system to reduce further shock wave and expansion fan interaction during release.

After the release of the Falcon 1 from the fuselage of the SARRA vehicle, the aerodynamics of the aircraft may change due to shifts in the static margin and the significant void in the body of the aircraft. The centers of gravity of the aircraft and payload are co-located to prevent changes in handling characteristics. A large void in the body of the aircraft leads to a drastic rise in base drag on the fuselage. To address this potential problem, the design employs inflatable balloons that reduce the gap in the fuselage and smooth out the void. With the balloons deployed after the release of the Falcon 1, the risk for base drag is significantly mitigated.

**Mission Profile.** The mission profile is developed based on the demands of the previously stated performance requirements, with consideration taken into account for the limitation of each component of the aircraft as well as the overall goals of reduced cost. A

visual representation of the mission profile is presented in Fig 3.

The entire mission process begins at the Kennedy Space Center, where the SpaceX Falcon 1 is loaded and attached to the vehicle and the LOX is loaded onto the rocket and aircraft. The SARRA vehicle takes off from climbs and accelerates to Mach 0.8 without the use of afterburners. At an altitude of 35,000 ft (10,670 m), the SARRA vehicle will initiate afterburners to break through Mach 1. At Mach 1.2, the SARRA vehicle will continue to climb utilizing the afterburners to an altitude of 50,000 ft (15,240 m) at a maximum velocity of Mach 2.25. After reaching this altitude, the vehicle begins the launch sequence. When the rocket is launched, the vehicle rapidly decelerates descends and returns to Kennedy Space Center.

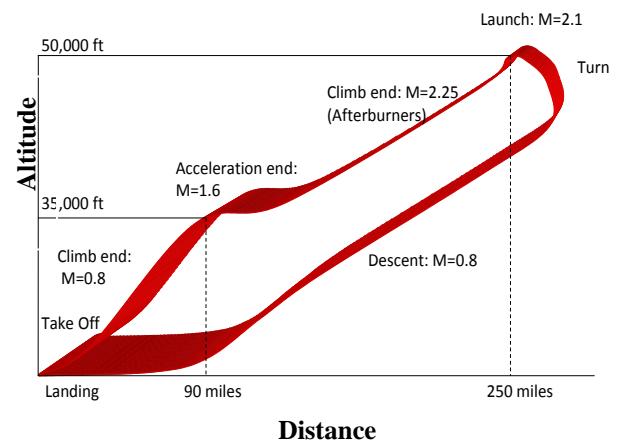


Figure 3. Mission Profile.

**Launch Sequence.** The release of the Falcon 1 requires a 4-step procedure. First is the commencement of a 25 deg pull-up maneuver into a parabolic aircraft flight trajectory, placing the Falcon 1 into ballistic flight at the moment of release. Second, the Falcon 1 is released from its support points and ejected backwards along rails. After the rocket is moved to 5% aircraft static margin, the rails retract and the Falcon 1 is then free of the aircraft. Third, no longer attached to the rocket, the aircraft commences a negative 1 g maneuver away from the Falcon 1. Finally, when the SARRA vehicle is clear of the Falcon 1, the CDD on the Falcon 1 deploys, giving the rocket pitch and yaw stability and eliminating the potential risk of oscillations until the engines achieve full thrust. Simultaneously on the SARRA vehicle, the balloons inflate into the void created by the absent Falcon 1, reducing any turbulence that may arise from the absence of the rocket.

**Surplus Fuel System.** Boil off liquid oxygen (LOX) is a major concern on the Falcon 1; however, due to the configuration of the fuel tanks, the only fuel that is boiled off is the LOX because the RP-1 is surrounded by the much cooler LOX. The rate of boil off for LOX is 8

gallons per minute (30 l/m) (Musk, 2005). One gallon of LOX is equivalent to 9.5 lb (4.3 kg) or 76 lb/min (35 kg/m) of boil off. The time from flight takeoff to rocket release is 29 minutes, bringing a total boil-off of 2204 lb (1000 kg). The SARRA vehicle carries a total of 4408 lb (2000 kg) of LOX aboard the aircraft. Due to the minor cost of LOX compared to the high cost of refrigeration, surplus LOX was decided upon as the method of choice for this operation. The liquid oxygen is pumped into the Falcon 1 beginning 10 minutes prior to the release sequence. There are two oxygen pumps onboard the SARRA vehicle, in the event the main liquid oxygen pump fails, the backup system automatically initiates. Conclusion of the LOX fueling coincides with the beginning of the release procedures. In the event of a mission abort, LOX is ejected through the rear of the aircraft.

**Summary of Operations.** Major areas of risk were identified and specific procedures and devices were developed to mitigate the identified risks. Development process allows the SARRA vehicle to deliver safely payloads for the customer. Furthermore, the SARRA vehicle's entire mission profile and rocket release procedure was developed and optimized to decrease the cost of operation. The logistics of development and manufacturing were also organized to minimize costs, making the SARRA vehicle economical.

### III. Configuration and Weights and Balance

Before any sort of analysis could begin, certain parameters were established for the SARRA concept. First, an initial sizing was conducted to establish the approximate gross take-off weight (GTOW) of the aircraft. Once this was ascertained, several basic concept designs were developed. These concepts were eventually narrowed down to a final three, on which a more in depth analysis was conducted. Finally, after investigations by each of the other specialists, the final concept was chosen.

Once the preliminary shape of the aircraft was established, a detailed build-up analysis was conducted based on individual component weights. This enabled a more accurate weight model for stability and control and structural analyses. Then, the internal configuration of the aircraft was designed to allow the needed CG shift during crucial parts of the flight. Finally, the CG during all portions of the flight was calculated.

**Initial Sizing and Concept Morphology.** The design of the SARRA concept began with an initial sizing to attain a preliminary weight of the aircraft. Equations 3.1-3.4, 3.6, 3.11, 6.9 and 6.22 as well as Fig 3.3 in Raymer were used for these calculations. Because details such as the lift to drag ratio (L/D) and the specific fuel consumption of the engines were as of yet unknown, several trade studies were conducted, altering the

variables to ascertain an average value of the weight. Based on these numbers, an initial weight of approximately 180,000 lb (81,646 kg) was attained.

Once an initial weight estimate was established, the next step was to start developing initial concept designs. Several of these designs are shown on the left side of Fig 4, which displays the concept morphology for our aircraft. Although additional factors were taken into account, the two main criteria used to evaluate each design were maximizing the aircraft's subsonic performance and the ability to travel at Mach 2 and higher. It was for this reason that many of the conventional wing aircraft were eliminated. Although it is possible to push a conventional wing to supersonic speeds, the amount of thrust required to push one to Mach 2 and above would unnecessarily increase the aircraft's cost enormously. With this in mind, the final three aircraft were selected and are shown in the center row of Fig 4. These concepts include a blended wing, a double delta wing, and a delta wing with canard. After a more detailed analysis of these three concepts by each of the specialists, the delta with canard was chosen.

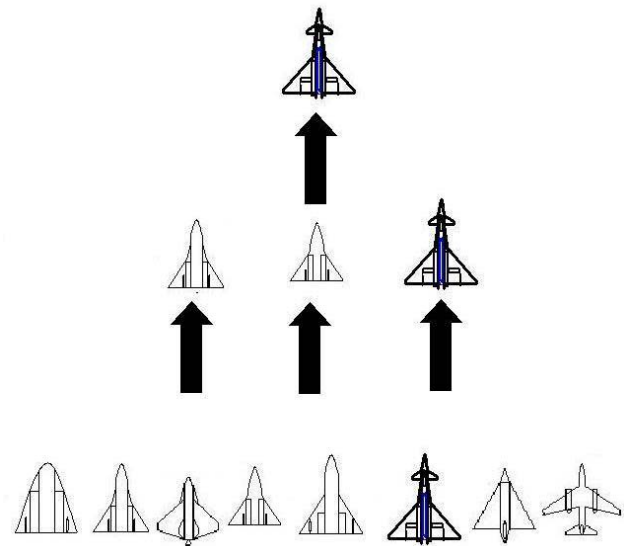


Figure 4. Concept Morphology

**Component Weight Analysis.** After the configuration had been chosen, a component weight analysis was conducted on the aircraft. Although an estimate of the GTOW was found in the initial sizing, a more in depth examination was necessary to find a more accurate GTOW as well as to enable the calculation of the center of gravity (CG). Using equations 15.1-15.45 in Raymer, the estimated weight of several aircraft components was calculated.

Because its performance characteristics resemble both a fighter and transport, weights modeled for both aircraft were used. For instance, because the control needed for the aircraft is most similar to a transport, the

weight for the control surfaces was modeled after a transport, but since the wing used on the aircraft is most commonly used on fighters, the weight estimate for a fighter wing was used. The only component that caused some difficulties was the estimate for the fuselage. The fighter estimate of 5,000 lb (2,270 kg) seemed too light, but the transport estimate of 25,000 lb (11,340 kg) appeared too heavy. Like a transport, a large portion of the aircraft's weight, including the entire payload, is located along the fuselage, but unlike a transport, the SARRA concept does not feature ringed bulkheads like a transport. These bulkheads are much weaker than a carry-through bulkhead and thusly require a much heavier structure. Because of the disparity between the fighter and transport weight estimates, a more in depth study was conducted on this particular component's weight. Two additional fuselage weight estimates were conducted using methods described by Corke (Corke, 2002) and Roskam (Roskam, 1987). These sources produced estimates of approximately 8,000 and 10,000 lb (3,630 and 4,536 kg) respectively, leading to the final estimate of 10,500 lb (4,760 kg). Figure 5 shows the weight of each category as a percent of the GTOW.

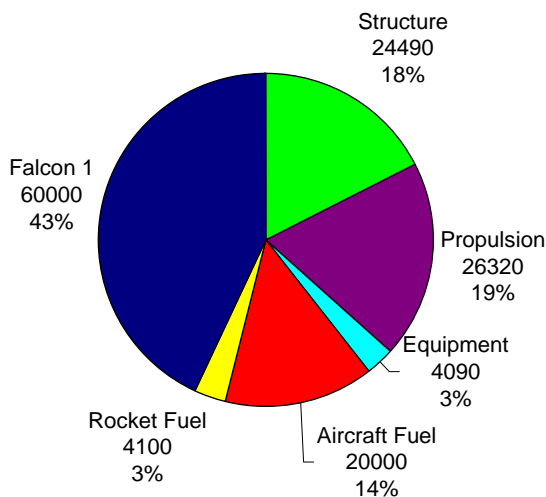


Figure 5. Category weights in pounds and as a percent of the Gross Take-off Weight

**Internal Configuration.** Once the weight was established, the internal configuration of the aircraft was determined. The purpose of the internal configuration is to provide approximate locations of internal components for the calculation of the center of gravity. Figure 6 shows the internal layout of the aircraft's major internal components.

Because some of the total internal volume of a section is used for structural support, a portion is not usable for internal storage. For instance, due to the relatively thin wings of the concept, much of its internal volume is given up to the structural supports. Therefore, 50% of the internal volume is available for fuel.

Likewise, to a lesser extent, since it is located in a location of less structural significance, the fuselage fuel tank has 92% of its internal volume available for fuel. Finally, the rocket fuel tank, which requires insulation, has 75% of its internal volume available for liquid oxygen.

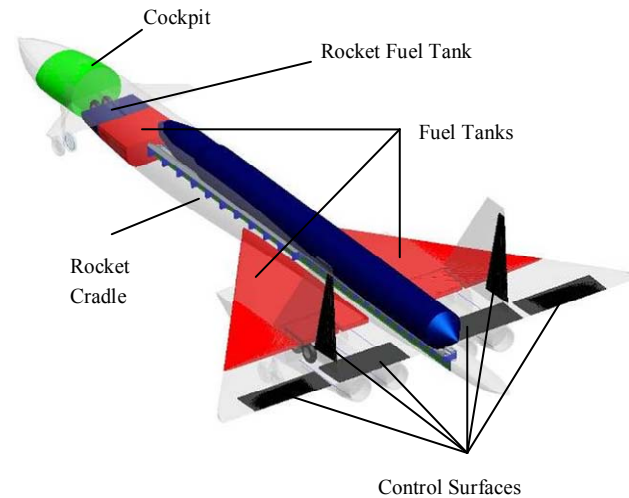


Figure 6. Internal layout of the SARRA concept

**Center of Gravity and Area Rule.** Once the location of each of these components was established, the center of gravity and moments of inertia were calculated. The goals for the center of gravity locations were as follows. For the majority of the flight, the ideal location of the CG is 68.5 ft (20.9 m) from the nose of the aircraft. Thus, upon take-off, fuel is burned only from the fuselage fuel tank until the CG is at this location. However, the moment the rocket is released from the aircraft, the CG has to be at 70 ft (21.3 m) from the nose, or coincident with the center of gravity of the rocket. To accomplish this, just prior to release, a small amount of fuel in the fuselage tank is pumped into the wing. After release, the fuel is pumped back into the fuselage fuel tank in order to return the CG to its optimum cruising location.

**Rocket Carriage and Release.** The Falcon 1 is carried in a semi-conformal cavity on top of the aircraft. Semi-conformal attachment was chosen as a means to reduce the drag over the rocket during flight. This reduction versus conventional carriage is mostly due to the removal of the external racks and pylons. Additionally, semi-conformal carriage grants an even greater reduction in drag due to the decrease in wetted area and in the maximum frontal area, which leads to a reduction in wave drag.

However, this type of carriage does have a cost. Due to research conducted on supersonic separation, it was decided that the shock behavior in the rocket storage cavity will likely cause a pressure differential along the length of the rocket causing it to pitch into the aircraft.

Shown in Fig 7, an expansion wave forms as the flow enters the cavity made by the vacant store.

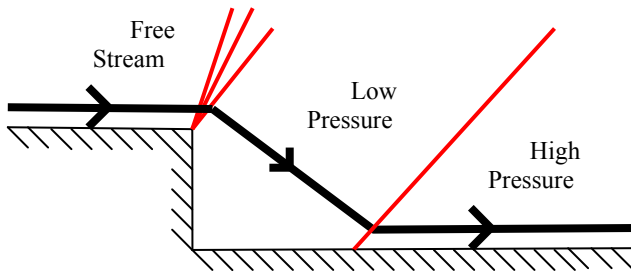


Figure 7. Supersonic Cavity Shock Interaction

The flow then passes through one or more shockwaves before expanding once again as it leaves the cavity. This series of expansion and shockwaves causes a low-pressure region at the front of the store and a high-pressure region at the rear of the store.

The factor that is most influential in determining the size of this differential is the length to height (L/H) ratio of the cavity. A larger ratio indicates a longer, thinner cavity that will allow greater flow interaction with the cavity floor and, in turn, will cause a greater pressure differential (Wilcox, 1991). An L/H ratio of 4 will still allow the store to separate normally, while a ratio of 10 will cause a moment great enough to cause the store to pitch toward the aircraft and a ratio of 13 can cause the store to cartwheel upon release. Although the cavity on the SARRA has a low L/H ratio of 4, the shock and expansion wave pattern over the cavity gives it a pressure differential typical of a cavity with an L/H ratio of about 10. This flow has a smaller pressure differential than other flow types, but still possesses a large enough pressure differential to make separation hazardous.

In order to counter the adverse pitching moment caused by the cavity's pressure differential, a passive venting system was installed in the floor of the cavity. Shown in Figs 8 and 9.

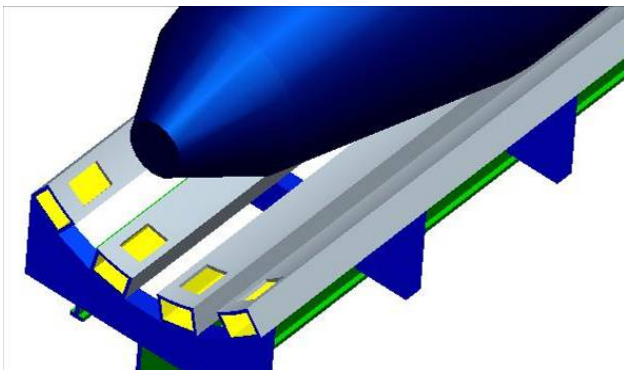


Figure 8. Front of Passive Venting System

This venting system uses the launching rails that were already present in the design as vent pipes that

transport high-pressure air from the rear of the cavity to the low-pressure area located at the front. This serves to decrease the pitching moment on the rocket and the drag caused by the cavity until the balloons have been inflated

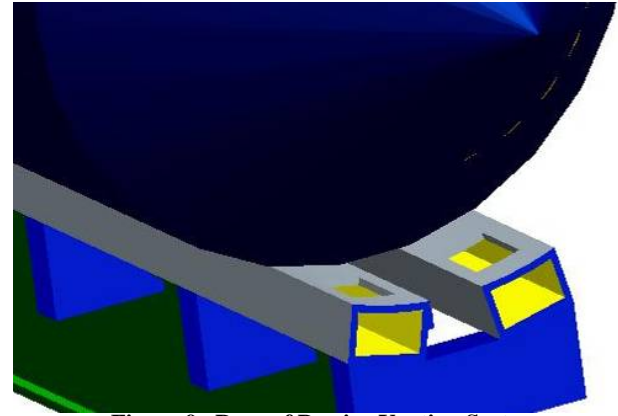


Figure 9. Rear of Passive Venting System

**Summary of Configuration.** The SARRA concept represents a lightweight and cost-effective solution to the problem of air-launch delivery. The delta wing design decreases structural weight while improving supersonic performance. It carries the LOX necessary to ensure that the Falcon 1 is fully fueled at the time of launch, as well as enough aircraft fuel to carry several different payloads. Its internal configuration allows the necessary change in the CG throughout the flight as well as ensuring that the rocket can separate safely from the aircraft. In short, the configuration of the SARRA concept meets or exceeds all of its expectations.

#### IV. Performance

Performance constraints for the SARRA launch vehicle include an outgoing range of at least 200 miles, a minimum ceiling of 50,000 ft (15,240 m), a payload compatibility with the 60,000 lb (27,200 kg) Falcon 1 rocket, and a maximum speed of at least Mach 2 upon release. Additional analysis of mission parameters, including the rocket separation maneuver, designates a required Mach 2.25 dash at 50,000 ft (15,240 m), a maximum material heating Mach limit of 2.45, takeoff distance of less than 15,000 ft (4,570 m), and additional payload capacity to accommodate 29 minutes of LOX rocket propellant losses due to boil off. This section will provide a detailed analysis of each mission requirement and the ability of the SARRA vehicle to meet or exceed it.

**Initial Design Point.** During preliminary aircraft constraint evaluation, minimum thrust-to-weight ratios are calculated over a range of structural wing-loading values for various mission segments, including takeoff, cruise, service-ceiling operation, dash, and landing. After curves for each mission segment are calculated, values are

normalized to sea level conditions and an optimal design point is chosen to meet all performance objectives. Limiting characteristic equations for the SARRA mission were found to occur during dash and takeoff segments.

$$\text{Takeoff: } \left(\frac{T}{W}\right)_{\text{TAKEOFF}} = \frac{(W/S)}{(TOP)\sigma C_{L_{TO}}} \quad (2)$$

$TOP$  = Takeoff Parameter

$C_{L_{TO}}$  = Takeoff Lift Coefficient

$\sigma$  = Density Ratio

$$\text{Dash: } \left(\frac{T}{W}\right)_{\text{DASH}} = \frac{q_{\infty} C_{D_o}}{(W/S)} + \frac{(W/S)}{q_{\infty} \pi e_o AR} \quad (3)$$

$q_{\infty}$  = Dynamic Pressure

$e_o$  = Span Efficiency

$AR$  = Aspect Ratio

$C_{D_o}$  = Dash Drag Coefficient

Figure 10 shows a general approximation for the initial design point of the SARRA vehicle, with a thrust-to-weight ratio of 0.55 and a wing loading of 155 lb/ft<sup>2</sup> (7,420 N/m<sup>2</sup>). However, a more detailed analysis is required to determine exact performance constraints and requirements.

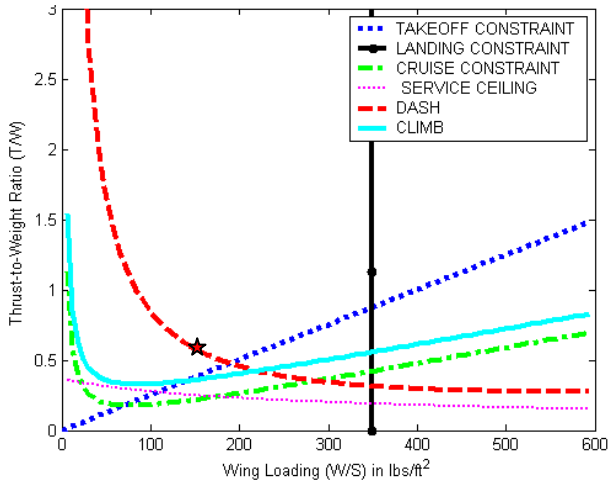


**Figure 10. Initial design point constraint diagram (T/W vs. wing loading)**

**Rocket Separation Trade Study.** The launch segment of the SARRA mission is the most physically demanding in terms of altitude and velocity requirements, so it provides a logical starting point for various performance constraint derivations, including minimum dash Mach number. Due to poor engine performance at 50,000 ft (15,240 m), the SARRA vehicle is unable to sustain an aggressive Mach 2.0, 25 deg climb. This

requires understanding aircraft deceleration and other velocity losses to the rocket.

Accelerating the rocket backwards along a rail system (while maintaining a positive aircraft static stability margin of at least 5%) will greatly reduce the risk of rocket to aircraft collision, but creates additional velocity losses. Therefore, a tradeoff between a long, slow separation (low ejection losses, high aircraft deceleration losses) and a short, sudden separation (high ejection losses, low aircraft deceleration losses) was studied. This tradeoff is explored in Fig 11, which shows that the optimal rocket separation takes place over a window of 2 s with a minimum overall velocity loss of 235 ft/s (71.6 m/s).

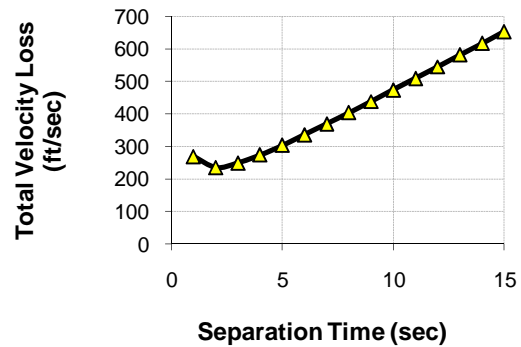


**Figure 11. Rocket separation trade study showing velocity losses vs. time at 50,000 ft.**

Once it is clear of the aircraft, the Falcon 1 slows further due to drag on the rocket and the CDD during the 4 s engine firing sequence. This component is relatively independent of separation time and is not used in the trade study.

By adding velocity losses of 235 ft/s (71.6 m/s) to the minimum Mach 2.0 rocket launch, (1,936 ft/s at 50,000 ft or 590 m/s at 15,240 m) a new minimum dash requirement of Mach 2.25 is calculated. This dash requirement could potentially decrease if aircraft deceleration was reduced below the current approximation of  $-36.84 \text{ ft/s}^2$  ( $-11.23 \text{ m/s}^2$ ) during a 25 deg climb at Mach 2.0 at 50,000 ft (15,240 m) altitude. This is achieved by decreasing aircraft weight, decreasing drag, or increasing available thrust.

**Performance Envelope.** The operational velocity range of the SARRA vehicle at a given altitude depends on stall speed, available thrust, drag, and surface temperature. Drag and available thrust are determined from tabulated aerodynamics and propulsion data for each altitude and Mach number. Stall speed is calculated according to the equation,

$$W = L = \frac{1}{2} \rho V_{\text{stall}}^2 SC_{L_{\text{max}}} \quad (4)$$

In Fig 12, values for  $V_{min}$  are determined by either the stall speed or the *lowest* velocity at which available thrust is equal to drag (the larger of the two values is chosen).  $V_{max}$  is shown as the greatest velocity at which available thrust is equal to drag. The materials limit designates the maximum velocity at any given altitude for which the structural integrity of an aluminum structure (with titanium leading edges) is maintained. By self-imposing this constraint, we are able to avoid the use of stainless steel or titanium skin, significantly decreasing the cost and weight of the aircraft.

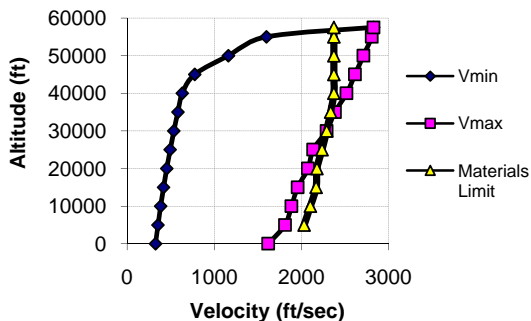


**Figure 12. SARRA vehicle performance envelope showing minimum and maximum velocities at altitude.**

The maximum aircraft operating condition during the dash segment is shown as 2,180 ft/s (663 m/s or Mach 2.25) at 50,000 ft (15,240 m). The absolute aerodynamic ceiling for this aircraft is 58,750 ft (17,900 m) at a velocity of 2,516 ft/s (767 m/s or Mach 2.6), but structural and material limitations reduce this to approximately 58,000 ft (17,680 m) at 2,370 ft/s (722 m/s) (Mach 2.45). The actual SARRA launch profile is well within the performance envelope at all times, confirming that the ceiling and maximum velocity capabilities of the SARRA vehicle exceed mission requirements.

**Takeoff Analysis.** In order to launch successfully from the John F. Kennedy Space Center in Cape Canaveral, Florida, the SARRA vehicle must demonstrate the ability to accelerate, rotate, transition, and climb to clear a 50 ft (15.25 m) obstacle within a 15,000 ft (4,570 m) runway. During ground roll, average acceleration is determined by vehicle mass and the sum of thrust, drag, and rolling frictional forces as expressed in the equation,

$$a = \frac{g}{W} [T - D - \mu(W - L)]_{\left(\frac{v_{TO}}{\sqrt{2}}\right)} \quad (5)$$

(Note that aerodynamic properties in this equation are evaluated at a velocity equal to  $V_{TO}/\sqrt{2}$ , where takeoff velocity  $V_{TO}$  is defined as  $1.1 * V_{stall}$  at sea level.

Kennedy Space Center elevation is ~10 ft above mean sea level.)

Based on Eq 5,  $V_{stall}$  at sea level = 314 ft/s (95.7 m/s) and  $V_{TO} = 346$  ft/s (105.5 m/s), meaning that lift and drag must be evaluated at a speed of 244 ft/s (74.4 m/s). Empirically, ground rolling resistance coefficient  $\mu$  is approximated as 0.05 for concrete and asphalt. Stationary thrust values at sea level are 43,639 lb (194 kN) without afterburners and 88,418 lb (393 kN) with afterburners. Assuming a minimal lift and drag configuration during ground roll acceleration, the parasite drag coefficient is approximated as 0.018 as lift approaches zero. For a GTOW of 145,000 lb (65,770 kg), this data yields a ground acceleration of 7.76 ft/s<sup>2</sup> (2.36 m/s<sup>2</sup>) without afterburners and 17.71 ft/s<sup>2</sup> (5.40 m/s<sup>2</sup>) with afterburners, covering runway distances of 7,688 ft (2,340 m) and 3,371 ft (1028 m), respectively, during the initial ground roll segment.

Since additional distance is required for transition and obstacle clearance, especially in the event of a tailwind, the SARRA vehicle will utilize afterburners during takeoff, much like the Concorde and other supersonic delta-wing aircraft. For a climb angle of 15 deg (maximum attainable takeoff climb angle is 26.5 deg), the transition segment ground distance will cover an additional 5,897 ft (1,800 m) of runway with a final altitude of 776 ft (237 m). Since this meets the 50 ft (15.25 m) obstacle clearance as per FAA takeoff regulations, no additional climb segment is required. Combining ground roll and transition segments, the total afterburning takeoff distance of the SARRA vehicle is 9,268 ft (2,825 m), which is below the 15,000 ft (4,570 m) requirement of Kennedy Space Center, as well as the 10,000 ft (3,048 m) runway maximum for many commercial airports, offering enhanced mission versatility.

**Dash Operation.** Figure 13 demonstrates values for drag, afterburning thrust, and non-afterburning thrust at 50,000 ft (15,240 m) altitude for various Mach numbers.

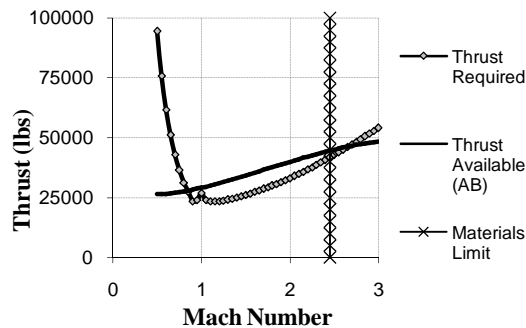


**Figure 13. Dash thrust required and available at 50,000 ft altitude.**



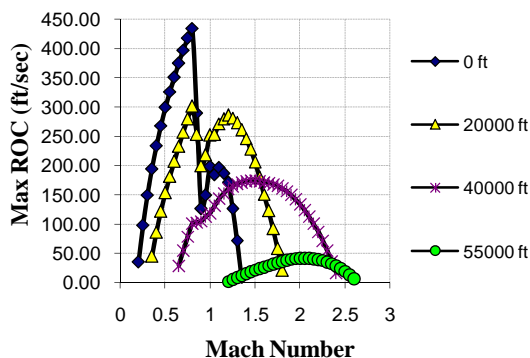
At the launch altitude of 50,000 ft (15,240 m), thrust losses approaching 70% (w.r.t. sea level thrust) present a challenge when attempting to accelerate or climb. A maximum material temperature constraint of Mach 2.45 has been placed to maintain structural integrity.

Figure 13 demonstrates that the aircraft can operate and accelerate at 50,000 ft (15,240 m) for Mach numbers ranging from 0.85 to 2.45, but excess thrust limitations have made it desirable to accelerate to Mach 2.25 at lower altitudes.

#### Service Ceiling and Maximum Rate of Climb.

Aircraft service ceiling altitude is conventionally defined as the altitude at which the maximum rate of climb is 100 ft/min (0.51 m/s). Figure 14 shows the rate of climb for various altitudes and Mach numbers assuming a gross takeoff weight of 145,000 lb (65,770 kg), as defined by the equation,

$$ROC_{\max} = \frac{VT_x}{W}. \quad (6)$$



**Figure 14. Maximum rate of climb at altitude, Mach number (weight = GTOW = 145,000 lb).**

By extrapolating the data in Fig 14, one can determine that the service ceiling of the SARRA vehicle at Mach 2.25 is approximately 57,500 ft (17,526 m). The absolute ceiling, as discussed previously (see Fig 12), was established at 58,000 ft (17,678 m) due to aerodynamic and material temperature constraints. During the rocket release maneuver, the aircraft achieves a maximum altitude of 51,810 ft (15,790 m) at Mach 2.0. Although this is below the service ceiling, thrust constraints limit the maximum sustainable climb angle to 2.4 deg without velocity losses. In order to achieve the required 25 deg climb angle during launch, aircraft momentum and deceleration were taken into account during the minimum dash velocity derivation, which shows that the pull-up launch maneuver is achieved from an initial speed of Mach 2.25. Since the SARRA vehicle has a maximum dash velocity of Mach 2.45 at 50,000 ft (15,240 m), its

ceiling and climb constraints are more than adequate to accomplish the mission.

**Mission Profile Analysis.** In accordance with modern flight optimization theory, the SARRA vehicle mission profile was established using the “Energy Altitude” method, which is used to maximize the efficient use of kinetic, potential, and chemical energy within the aircraft. According to this analysis method, fuel-to-climb is minimized when the term  $P_x/c_t T$  is maximized. Since turbofans operate most efficiently at full power,  $c_t$  was fixed at 0.562 lb/hr/lb (0.0573 kg/hr/N) for non-afterburning mission segments and 2.46 lb/hr/lb (0.2508 kg/hr/N) during afterburning mission segments. The only exception was the descent mission segment, when the partial power operation equation was used.

$$\frac{c_t}{c_{\max dry}} = \frac{0.1}{\left(\frac{T}{T_{\max dry}}\right)} + \frac{0.24}{\left(\frac{T}{T_{\max dry}}\right)^{0.8}} + 0.66\left(\frac{T}{T_{\max dry}}\right)^{0.8} + 0.1M \left[ \frac{1}{\left(\frac{T}{T_{\max dry}}\right)} - \left(\frac{T}{T_{\max dry}}\right) \right] \quad (7)$$

At each altitude, available thrust and drag were compared at each Mach number to determine the operating velocity which provides maximum excess power (See Appendix B). These flight conditions were used to create an optimal climb profile in which the aircraft gradually accelerates such that it is operating at the ideal Mach number for each altitude (the notable exception being the horizontal segment at 35,000 ft (10,670 m), during which the aircraft crosses the sound barrier). Between each point in the profile, climb angle was chosen such that time-to-climb from Altitude ‘A’ to Altitude ‘B’ was equal to time-to-accelerate from Optimal Velocity ‘A’ to Optimal Velocity ‘B’, minimizing segment fuel consumption. Fuel used for each mission segment was calculated according to the equation,

$$W_f = \frac{c_t T t}{3600}. \quad (8)$$

Once this analysis was completed, it was determined that the distance required to climb to 50,000 ft (15,240 m) and accelerate to Mach 2.25 with minimal fuel consumption was 359 miles (577 km), far greater than the outgoing requirement of 200 miles (322 km). Rather than flying in a straight eastward path, a “spiral” climb, designed so that the rocket launch occurs at a point 250 miles (402 m) offshore, would shorten the return mission segment by more than 100 miles (160 km), resulting in a fuel savings of 1,908 lb (865.5 kg).

Figure 15 shows a detailed outline of the final mission profile, which has a total range of 660 miles (1,062 km). Total fuel consumption is approximately 18,250 lb (8,278 kg) from takeoff to landing and mission duration is 60 minutes. Table 1 shows a more specific breakdown of distance, duration, and fuel consumption for each mission segment. Time from takeoff to rocket launch is approximately 29 minutes, allowing one to approximate the amount of additional LOX propellant required to counteract boil off. Alternatively, the SARRA vehicle can be used to transport its payload between ground locations, offering a maximum ferry range of over 775 miles (1,247 km).

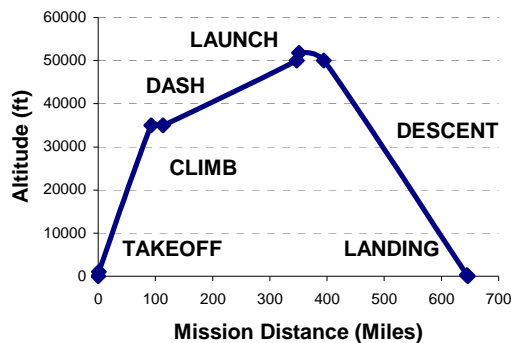


Figure 15. Final mission profile (altitude vs. range).

Table 1. Mission Segment Duration, Fuel Consumption, and Horizontal Distance

Mission Segment	Time (s.)	Fuel (lb)	Distance (ft)
Takeoff	27	712	9,267
Climb & Accelerate to Mach 0.8	634	3,515	483,019
Level Dash to Mach 1.8	150	5,296	180,621
Climb + Accelerate to Mach 2.25	910	3,807	1,233,226
Launch Rocket	10	297	21,780
Turn	196	530	228,017
Descent	1,604	4,026	1,320,157
Landing	40	48	9,921
<b>Total</b>	<b>3,572</b>	<b>18,231</b>	<b>3,486,009</b>

**Summary of Performance Data.** After a detailed performance analysis of the SARRA vehicle, it is evident that the aircraft meets or exceeds all mission requirements. To achieve a  $\Delta V$ -to-orbit reduction of 4,593 ft/s (1,400 m/s), the aircraft releases the Falcon 1 rocket at Mach 2.0 during a decelerating 25 deg climb at a peak altitude of 51,810 ft (15,790 m). To accommodate aircraft deceleration and other velocity losses during the

release segment, excess thrust at 50,000 ft (15,240 m) is sufficient to achieve a Mach 2.25 dash. After examining aerodynamic and self-imposed structural constraints, it was concluded that the maximum operating limit of the aircraft is well beyond the mission requirements with an absolute ceiling of 58,000 ft (17,680 m) at a velocity of 2,372 ft/s (723 m/s or Mach 2.45). This material limit allows us to use a predominantly aluminum structure with titanium leading edges, avoiding costlier and heavier alternatives, such as stainless steel. Using afterburners during takeoff, the SARRA vehicle is able to operate using a 10,000 ft (3,048 m) runway available at many major commercial airports, as well as the Kennedy Space Center. By applying the governing equation of the “Energy Altitude” method and a spiraling climb strategy, a mission profile was established which requires approximately 18,250 lb (8,280 kg) of fuel, lasts 60 minutes, and covers a range of 660 miles (1,062 km). This unique combination of performance, versatility, and cost-effectiveness makes the SARRA vehicle an attractive platform for a reusable rocket launch with the potential to revolutionize space accessibility.

## V. Aerodynamics

The aerodynamic design of the SARRA concept vehicle is critical to performance and mission success. Any supersonic air launch system must perform well at both subsonic and supersonic flight as well as withstand the demands of a high Mach number rocket air launch.

A summary of the important aerodynamic characteristics of the SARRA concept vehicle appears in Table 2 for two operating conditions. The following section will address the major aerodynamic design elements of the SARRA vehicle.

Table 2. Summary of Aerodynamic Properties of the SARRA Vehicle at  $M = 0.80$  and  $M = 2.00$

Condition	Mach 0.80 at sea level	Mach 2.00 at 50,000 ft
$S_{ref}$ (ft <sup>2</sup> )	1174	1174
Wingspan (ft)	59.4	59.4
$C_{D0}$	0.0208	0.0339
K	0.2021	0.4598
$C_L$ required for level flight ( $W=145,000$ lb)	0.12	0.18
$C_D$ for level flight ( $W=145,000$ lb)	0.210	0.0416
$C_{L\alpha}$ (per deg)	0.057	0.041
$L/D_{max}$	12	6.6

**Wing Geometry Selection from Trade Study Results.** Important aerodynamic considerations during the design of the SARRA vehicle were the selection of the wing planform, wing thickness, aspect ratio, and sweep angle. Each of these parameters was chosen with an overall goal of increasing aerodynamic efficiency and thus decreasing cost.

A delta wing planform was chosen for its simplicity and the fact that it is a proven supersonic wing design. A historical trade study of existing supersonic aircraft was performed with specific interest in large supersonic delta wing aircraft such as the XB-70 and Concorde. Maximum wing thicknesses of these existing aircraft were found to be around 2-3% of their chord (Lednicer, 2006). Data from Hall (1953) showed that a thin wing decreases supersonic drag and results in an increased drag divergence Mach number. Based on the historical trade study and supporting data the maximum wing thickness of the SARRA vehicle was chosen as 3% of its chord.

In order to determine the most efficient aspect ratio, delta wings with aspect ratios ranging from 2 to 4 were studied using existing test data. The key aerodynamic parameters examined were maximum lift to drag ratio  $L/D_{max}$ , maximum lift coefficient  $C_{L,max}$ , and the induced drag coefficient  $K$ .

An important indicator of aerodynamic efficiency is  $L/D_{max}$ . Test data (Hall, 1953) seen in Fig 16 shows that as aspect ratio increases  $L/D_{max}$  increases (higher efficiency) for speeds less than Mach 1. At speeds greater than Mach 1 the effect of aspect ratio on  $L/D_{max}$  was negligible.

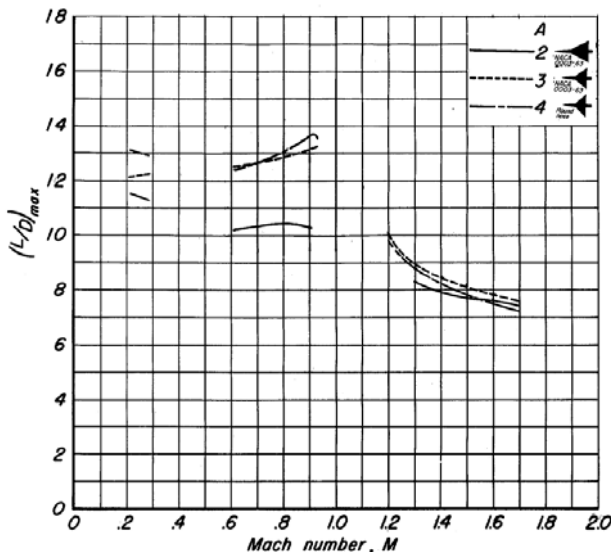


Figure 16.  $L/D_{max}$  vs. Mach number for delta wings of AR = 2, 3, and 4 (Hall, 1953).

Another important consideration is that the wing planform area remains inside the Mach cone in order to avoid excessive drag at supersonic speeds. The wing

aspect ratio was set as large as possible without interfering with the Mach angle created at a maximum Mach number of 2.5. The larger aspect ratio increases  $L/D_{max}$  and decreases induced drag at Mach numbers less than 1. The resulting wing planform of the SARRA vehicle has a sweep angle of 53.1 deg and an aspect ratio of 3.

**Airfoil Selection – NACA 64-103.** A cambered airfoil was chosen in order to reduce induced drag and increase aircraft performance at subsonic speeds. A NACA 6-series airfoil was chosen based on a historical survey of existing supersonic aircraft and their airfoils (Lednicer, 2006). A design lift coefficient of 0.1 was selected for minimum drag during the climb and dash segments of the mission. The selected airfoil maintains its minimum drag at lift coefficients from 0 to 0.2.

**Drag Breakdown at Subsonic Speeds.** The methods for estimating subsonic drag relied largely on techniques found in Roskam (1989) except for the wing drag coefficient. Data from Hall (1953) showed drag for a wing body combination as well as drag for the body alone. From these two cases, wing drag was estimated by subtracting the drag of the body alone from the total wing body drag. Drag of the fuselage and control surfaces (canards and tails) was assumed to be mostly skin friction drag with an extra 5% estimated for leakage and protuberance drag, trim drag, and base drag. A summary of subsonic drag appears in Table 3.

Table 3. Drag breakdown at  $M = 0.5$  and standard sea level conditions

Component	Component Description	$C_{D0}$ (based on $S_{ref}$ )	Percent of $C_{D0}$
Wing	53.1 deg leading edge sweep delta wing, $A = 3$	0.0038	19%
Fuselage and Engines	120 ft long, 8 ft diameter	0.0130	64%
Rocket	70 ft long, 5.5 ft diameter	0.0013	6%
Canards	Tapered control surface	0.0003	1%
Tails	45 deg vertical sweep	0.0009	4%
Misc.	Leakage and protuberances, trim drag, base drag	0.0010	5%
	PARASITE GEAR UP:	0.0202	
Landing Gear	Nose: 2 tires side by side, Main: 4 tires in tandem configuration	0.0019	-
	PARASITE GEAR DOWN:	0.0221	
Induced Drag	Mach 0.5 at $CL = 0.33$ required for level flight	0.0258	-
	TOTAL $C_D$ GEAR UP:	0.0460	
	TOTAL $C_D$ GEAR DOWN:	0.0479	

The gear up parasite drag coefficient of 0.0202 is roughly twice as large as the XB-70 parasite drag coefficient (Arnaiz, 1977) but this is expected considering an externally carried rocket and the larger fuselage necessary for supporting it.

**Drag Breakdown at Supersonic Speeds.** Drag at supersonic speeds was estimated much in the same way as subsonic drag with the exception of the use of supersonic missile data (Piland, 1954) to estimate the fuselage drag. The appearance of wave drag was modeled using Roskam (1989). The total supersonic drag at Mach 2.0 and 50,000 ft (15,240 m) is summarized in Table 4.

**Table 4. Drag Breakdown at M = 2.0 and 50,000 ft standard conditions**

Component	Component Description	Component $C_{D0}$ (based on $S_{ref}$ )	Percent of $C_{D0}$
Wing	53.1 deg leading edge sweep delta wing with $A = 3$	0.0074	22%
Fuselage and Engines	120 ft length with max. diameter of 8 ft	0.0149	44%
Rocket	70 ft length with max. diameter of 5.5 ft	0.0011	3%
Canards	Tapered control surface	0.0002	1%
Tails	45 deg sweep vertical control surface	0.0007	2%
Wave Drag	-	0.0078	23%
Misc.	Leakage and protuberances, trim drag, base drag	0.0016	5%
	PARASITE:	0.0337	
Induced Drag	Mach 2.0 at $C_L = 0.18$ required for level flight	0.0078	-
	TOTAL $C_D$ :	0.0415	

**Parasite Drag vs. Mach Number.** A summary of the parasite drag coefficient versus Mach number for the SARRA vehicle is shown in Fig 17. The transonic region (above the drag divergence Mach number of 0.80 and below Mach 1.2) was estimated using XB-70 data (McCormick, 1995). The ratio of the XB-70 parasite drag at Mach 1 to the drag at Mach 0.8 was used to estimate the transonic drag rise.

**Lift Curve Slope  $C_{L\alpha}$ .** The lift curve slope  $C_{L\alpha}$  was obtained from wing test data (Hall, 1953) for a delta wing with aspect ratio 3. The resulting  $C_{L\alpha}$  versus Mach number plot appears in Fig 18. The lift curve slope increases with subsonic Mach number and decreases with supersonic Mach number as expected (McCormick, 1995).

**Pitching Moment  $C_{m\alpha}$ .** Pitching moment about the mean aerodynamic center versus lift coefficient was

obtained using wing data for a delta wing with aspect ratio 3 (Heitmeyer, 1951).

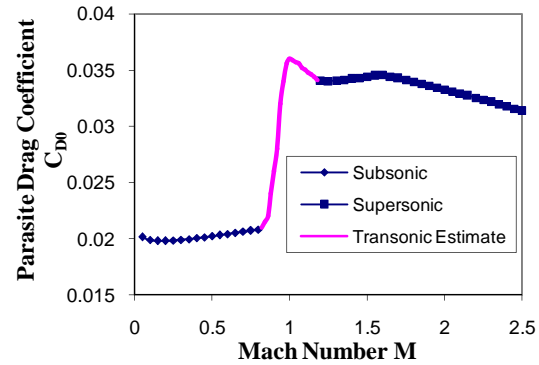


**Figure 17. Parasite drag vs. Mach number.**

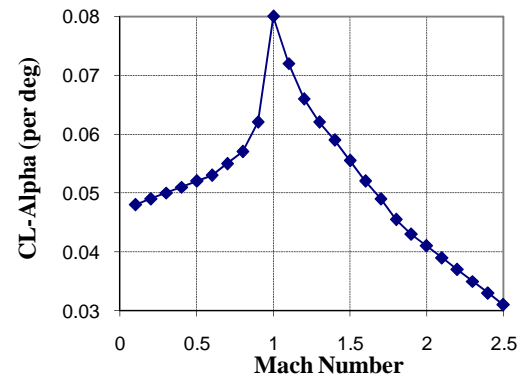


**Figure 18. Lift curve slope versus Mach number adapted from Hall (1953).**

**Drag Polars and  $C_{Lmax}$ .** Using the induced drag coefficient, parasite drag coefficients, and  $C_{L\alpha}$  values from previous sections, drag polar plots were created for various Mach numbers. The drag polar was modified to reflect the addition of camber by offsetting the induced drag by 0.1 (the design lift coefficient of the airfoil). The drag polar equation used was

$$C_D = C_{D0} + K(C_{L\alpha}\alpha - 0.1)^2 \quad (9)$$

The drag polar curves are plotted in Fig 19. These plots were used to estimate  $L/D_{max}$ .

**Maximum Lift Coefficient  $C_{Lmax}$ .** Maximum lift coefficient was estimated using delta wing test appearing in McCormick (1995). Table 5 shows the maximum lift coefficient and stalling angle of attack for three Mach numbers. Due to the SARRA vehicle's high thrust availability, the  $C_{Lmax}$  of 1.05 was large enough to ensure adequate takeoff performance without the use of high lift devices.

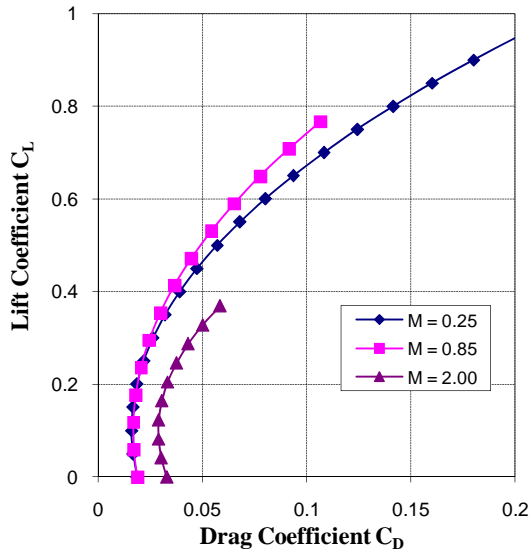


Figure 19. Drag Polars for  $M = 0.25, 0.85, \text{ and } 2.00$ .

Table 5.  
Maximum Lift Coefficient and Stalling Angle of Attack

Mach Number	$C_{L,max}$	$\alpha_{stall}$ (deg)	Source/Method
0.25	1.05	19.4	(McCormick, 1995) Fig. 3.78

**Summary of Aerodynamics.** The SARRA vehicle was designed to be aerodynamically efficient in order to increase performance and reduce mission cost. Based on trade studies subsonic  $L/D_{max}$  was maximized by setting the leading edge sweep angle to 53.1 deg while still remaining inside the Mach angle created by the nose of the fuselage. A cambered airfoil was used to decrease induced drag. Drag coefficients, induced drag factors, lift curve slopes, and wing-pitching moments were obtained from real world data to provide an accurate estimation of aircraft performance.

## VI. Propulsion

For the SARRA vehicle to meet its design goals, a powerful and efficient propulsion system is required. The most important part of the propulsion system is the engine. To choose an engine, several existing engines with the power necessary for the mission were examined and the one that was the most efficient was chosen. Existing engines were studied because they would require no development costs and the methods for servicing them as well as their performance characteristics are well known. Once selected, an engine performance analysis was made. This included determining the partial power specific fuel consumption and the thrust losses due to

installing the engines on the SARRA vehicle. The configuration of the engines also had to be determined, and this required the inlet capture area and the length of the diffuser. Once the inlet configuration and type were decided upon, the geometry of the inlet was designed. This included determining the angles of the ramps that would yield the best pressure recovery at various Mach numbers. Finally, the engine fuel system was designed.

**Engine Selection.** Originally, there were four candidates for the engines to power the SARRA vehicle. They were the F100-PW-229, the F101-GE-102 (Fig 20), the F110-GE-100, and the Olympus 593 Mk 610. The first three are afterburning low bypass turbofans and the last one is a turbojet. These engines have all been in service for years, are all proven designs, and require no development. All of these engines met the total thrust required of 102,000 lb (454 kN) of thrust with four engines (Table 6).

Table 6. Thrust and SFC Data (Mattingly)

Engine	Max Thrust (lb)	SFC (1/hr)	Afterburning SFC (1/hr)
F100-PW-229	29000	0.74	2.05
F101-GE-102	30780	0.562	2.46
F110-GE-100	28620	1.47	2.08
Olympus 593 Mk 610	38050	1.19	1.39

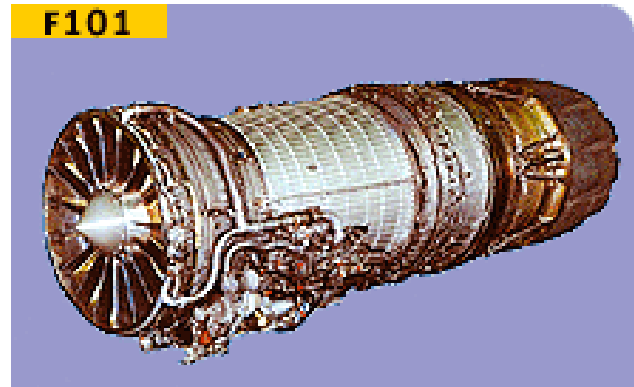


Figure 20. The F101-GE-102 engine (Meier, 2005).

Since all of the engines met the thrust requirement, the selection came down to the specific fuel consumption or SFC. After doing a sizing analysis, it was determined that the craft would use the least amount of fuel with the F101-GE-102. This reduction in fuel used translates directly into a lower operating cost. Thus, the F101-GE-102 is the engine that powers the SARRA vehicle.

**Inlet, Nozzle, and Diffuser Size.** Once the engine was chosen, the size of the inlet and the length of the diffuser were determined. This was done using Eq 10.

$$A_{\text{inlet}} = \left[ \frac{m \left( 1 + \frac{m_s}{m} \right)}{\rho_{\infty} V_{\infty}} \right] \left( 1 + \frac{A_B}{A_C} \right) \quad (10)$$

This equation has been slightly modified from the one in Raymer due to an error in the equation. The inlet maximum area was found to be 16 ft<sup>2</sup> (1.49 m<sup>2</sup>) per inlet for a total area of 64 ft<sup>2</sup> (5.95 m<sup>2</sup>). This is important for determining the maximum area of the aircraft and for area distribution along the centerline, two concepts that heavily affect supersonic drag.

Another element that affects drag is the exit area of the nozzle. The exit area of the nozzle was determined from approximations in Raymer. For subsonic speeds, it was 8 ft<sup>2</sup> (0.743 m<sup>2</sup>) and at full afterburner, it is 19 ft<sup>2</sup> (1.77 m<sup>2</sup>). The nozzle adds drag to the aircraft and varies for the different nozzle settings. This is taken into account not as extra drag but rather as a loss to thrust and is examined in the installed thrust section. On the SARRA vehicle, a converging-diverging ejector nozzle is used to improve the efficiency of the nozzle. The cooler air that has been bled around the engine and sent out the ejector nozzle cools the nozzle and results in a fourfold increase in nozzle life.

The size of the diffuser is determined by having a balance between being long enough to ensure a slow increase in diameter to prevent separation and being short enough to prevent excessive boundary layer losses and to keep weight down. The diffuser length is 18 ft (5.49 m), a little less than four times the diameter of the engine face. This length is short enough to ensure a minimum of boundary layer losses but also prevents the flow from separating inside of the diffuser.

**Installed Thrust.** When installing an engine into an aircraft there are many losses involved. These include inlet pressure recovery, diffuser losses, compressor bleed, power extraction, nozzle efficiency, nozzle drag, and inlet drag. Of these, some take away more thrust than others do.

The inlet pressure recovery is the most important loss for a supersonic aircraft. At high supersonic speeds, the pressure recovery is poor due to shocks that the flow must pass through to get through the inlet. As the speed increases, the shocks get stronger so the pressure recovery decreases. To help reduce this effect the SARRA vehicle has a three-shock external compression inlet. The pressure recovery is greater through a series of oblique shocks than it is through a single normal shock. Having more shocks results in better pressure recovery. If more than three shocks are used, the inlet becomes overly complicated and often it does not have comparative gains. Figure 21 shows the pressure recovery for a 2-D three-

shock inlet. In the graph, the inlet is optimized for each Mach number.

As shown in Fig 21 the inlet chosen for the SARRA vehicle has a reasonably good pressure recovery since the SARRA vehicle will not operate at speeds above Mach 2.25. In order to get the pressure recovery shown in Fig 21, a variable ramp is needed, the cost of which is justifiable considering the performance benefit gained. This helps the pressure recovery and also the inlet drag or spillage drag, and ultimately reduces fuel burned and total cost.

In order to get a more accurate estimate of what the inlet will perform like a more detailed design of the inlet was performed. The inlet was designed using AEDSys

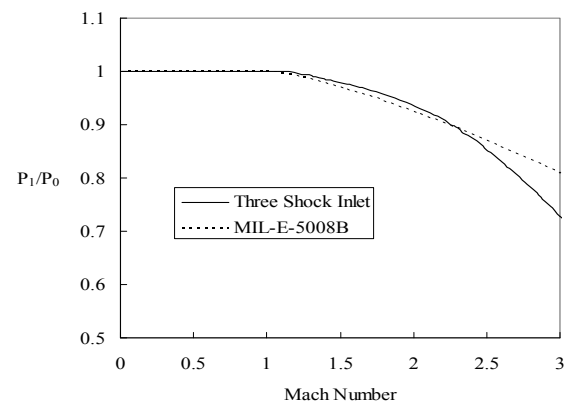


**Figure 21. Pressure Recovery varying with Mach number (adapted from Raymer).**

software (Mattingly, 2002). The design Mach number was set at 2.25 since that was the maximum speed the aircraft required during its mission. At that speed, the two ramps are set at 12 deg and 13.5 deg (Fig 22). This

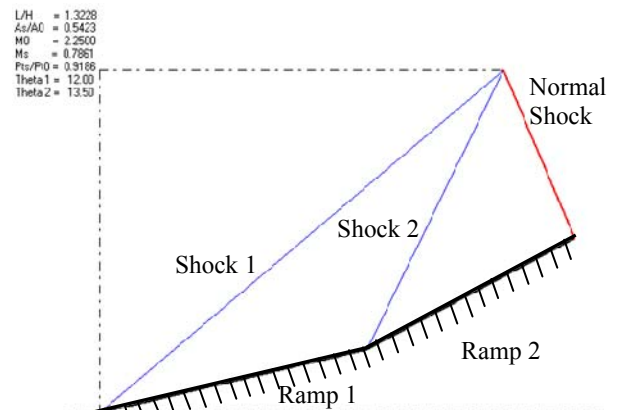


**Figure 22. Shock and ramp layout for the SARRA vehicle at M=2.25.**

yields a pressure recovery of 0.92, which is higher than the values that were adapted from Raymer. Once the design point was determined, a shock schedule was

determined to ensure maximum pressure recovery at every Mach number.

This schedule optimizes pressure recovery for all flight regimes. Figure 23 shows the pressure recovery from this ramp schedule as well as the ratio of the capture area to the capture area of the design Mach number. This capture area ratio shows how much of the air mass flow is not needed by the engine. This ratio can give a rough estimate of how much spillage drag occurs.

The spillage drag is caused by shocks not ending on the lip of the inlet cowl. This causes excess air to flow through the shock and then around the inlet. This large source of drag, if unaddressed at high speeds, can be up to 25% of the total drag on the aircraft. To avoid this in the SARRA vehicle the excess air is allowed to enter the inlet. Instead of going to the engine, the excess is bled off and sent around the outside of the engine to help cool the engine, afterburner, and nozzle. The air is then sent out the ejector nozzle. This reduces the drag to a low number that is equal to the momentum loss of the bleed air, but since it is sent out the nozzle and accelerated, the loss is small.

As the flow is expanded in the diffuser, losses are incurred through the boundary layer. Since the aircraft does not have excessively long or short diffusers, there are small boundary layer related losses and no separation. These losses have been reduced by changing the inlet layout from two inlets for four engines to an inlet for each engine. This eliminates the need to split the flow in the diffuser and thus any losses caused by the split.

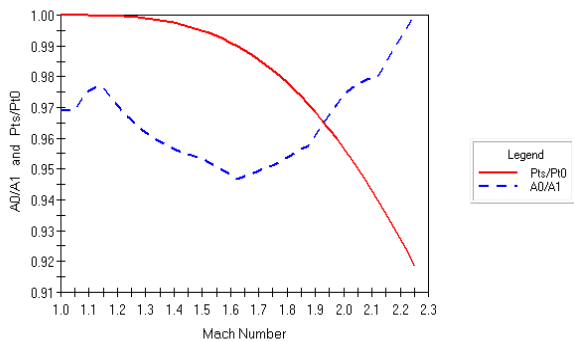


**Figure 23. Pressure recovery and capture area ratio for the SARRA versus Mach number.**

Compressor bleed can cause a large reduction in thrust. Compressor bleed is air that is taken out of the engine after the compressor for air conditioning and deicing purposes. This high-pressure air bleed causes an out of proportion thrust loss as Eq 11 shows.

$$\%thrustloss = C_{bleed} \left( \frac{\dot{m}_{bleed}}{\dot{m}_{engine}} \right) \times 100 \quad (11)$$

The bleed air is low because the SARRA has a small cockpit and deicers, minimizing the need for compressed air.

One factor that has a small effect on the thrust is power extraction. On an aircraft the only source of power are the engines, thus aircraft engines often power generators to run the electrical systems of the aircraft. They will also power the fuel pumps and hydraulic pumps for the aircraft. For the SARRA vehicle, the engines need to power a generator to supply electricity to the avionics. The engines also have to power the fuel pumps and the hydraulic pumps used for the landing gear and the control surfaces. The hydraulic pumps require about 107 hp (80 KW) of power. Each engine has 174 hp (130 KW) taken out, totaling 697 hp (520 KW) taken from the engines. This translates into about 100-200 lb (445-890 N) loss of thrust depending on the flight condition. This amount of power is more than sufficient for the systems on the SARRA vehicle.

The final loss caused by installing the engine in the aircraft is the drag caused by the nozzle. For an ejector nozzle, this drag is about 2.5% of the total drag. This results in a drag of about 100 lb (445 N) for subsonic flight and about 300-400 lb (1335-1780 N) for supersonic flight at altitude.

**Altitude Losses.** As the aircraft flies higher, a relatively large loss in thrust occurs. This is caused by the lower density at altitude. To model the loss of thrust Eq 12 was used.

$$\frac{T}{T_{sealevel}} = \left[ 0.88 + 0.245(M - 0.6)^{1.4} \right] \left( \frac{\rho}{\rho_{sealevel}} \right)^{0.7} \quad (12)$$

This equation also varies the thrust with speed. The reduction in density results in a reduction of mass flow to the engine, which produces a loss of thrust. An increase in speed has the opposite effect on the thrust. For subsonic speeds, however the thrust is almost constant regardless of speed. Figure 24 shows how the thrust varies with different flight conditions.

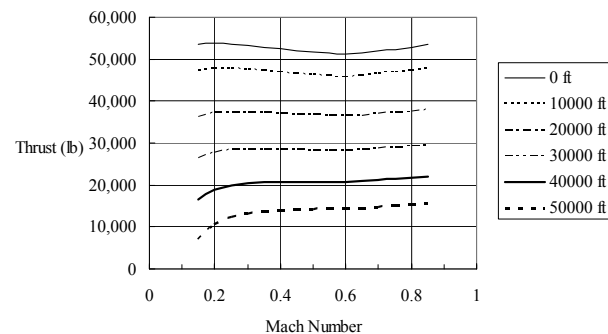


**Figure 24. Subsonic dry thrust at several different altitudes.**

The maximum thrust available is needed to calculate the partial power SFC. With the partial power SFC, an accurate model of the fuel burned during the mission was made.

**Specific Fuel Consumption.** As the aircraft performs its mission, the throttle setting will change and this causes a change in the SFC. If the engines are not operating at full power the SFC increases. This is caused by a reduction of thrust but not an equal decrease in fuel burn. To illustrate this Fig 25 shows the SFC for steady level flight at several altitudes.

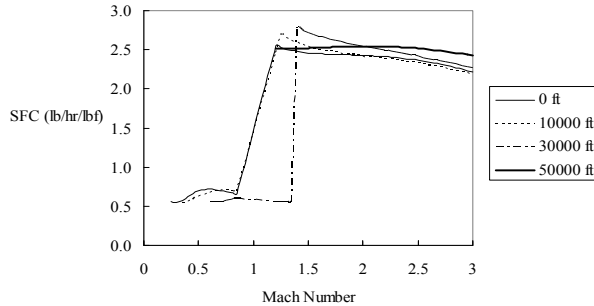


Figure 25. SFC varying with Mach number and altitude.

This thrust required for steady level flight is just the drag at each Mach number and altitude. This was obtained from the aerodynamics specialist. It illustrates that whenever excess thrust exists the SFC is larger than the full power value.

**Fuel System.** The fuel system is an important part of the aircraft, as it provides the engines with the fuel to operate. The primary fuel system consists of 3 integral fuel tanks, 2 feed tanks, 6 fuel pumps, and 9 valves. A schematic of the system is shown in Fig 26.

Integral fuel tanks were used to maximize the available volume for fuel as well as to reduce cost. Bladder tanks were unnecessary because self-sealing fuel tanks are excessive on an aircraft that is not going into combat. The tanks that are closer to the engines will contain foam that will prevent the fuel from leaking out of the tanks and perhaps causing a fire. This reduces the fuel volume by about 2.5% and traps some fuel in the foam. Fuel is stored in the feed tanks prior to being pumped to the engines. This ensures a continuous fuel supply to the engines. This ensures a continuous fuel supply to the engines for a period in case of a pump failure. This gives the backup pumps time to start up without the engines dying. It also provides fuel to the engines in case of a sudden throttle up so that the fuel is immediately available.

The pumps are capable of pumping fuel from the wing tanks to the fuselage tank to control the location of the center of gravity of the aircraft. The aircraft also has a pump used for dumping fuel if needed. The valves control where the fuel goes within the whole system. The feed tank pumps are driven by the engines through the

airframe mounted accessory drive (AMAD). The AMAD also runs all of the hydraulics for the aircraft. All of the pumps are ultimately driven by power extracted from the engine.

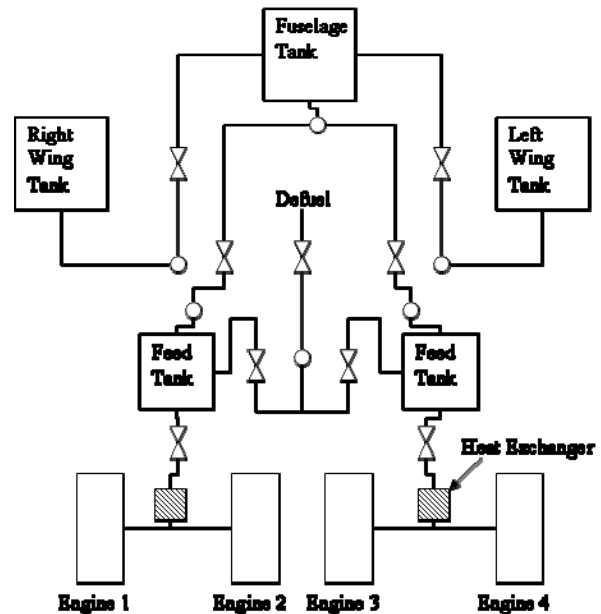


Figure 26. Fuel System Schematic.

There are also heat exchangers that use fuel as a heat sink to dissipate the heat from the engines preventing overheating. In case of an emergency, a T-62T-46-2 auxiliary power unit (APU) provides power for the hydraulics and avionics and fuel pumps. It is capable of providing 300 hp (224 kW) of power.

**Summary of Propulsion.** The F101-GE-102 was chosen for its ability to meet thrust requirements and its good fuel usage. It is also a proven design that will cut down maintenance costs. Then a model for how the engine will actually behave in the aircraft was created. This includes the installation losses, partial power SFC, as well as the changing thrust with altitude and Mach number. Once this was done the dimensions of the inlet and diffuser were determined to find a place for the engine in the aircraft. After the placement of the engines, the inlet was designed to provide the maximum possible pressure recovery while minimizing the expense. Finally, fuel was provided to the engines without changing the center of gravity too much, which might make the plane uncontrollable.

## VII. Stability and Control

As the SARRA concept calls for a high performance aircraft, strict optimization is a necessity. The stability of the SARRA vehicle, as well as its methods used for control were taken into consideration in order to create an aircraft that would satisfy both a low cost theme and



satisfy the performance requirements necessary to complete the SARRA mission.

**Design Morphology.** SARRA calls for an aircraft that can fly at high supersonic speeds and launch a rocket simultaneously. The aircraft must remain in control at all points during flight, and it is preferable that it remains statically stable as well.

In order to achieve this, a canard delta configuration was chosen, partially because of its success on previous supersonic designs, and for its own reasons. Some of these include better stall characteristics, an added amount of lift, and a larger allowable range of the center of gravity location. The center of gravity of the SARRA vehicle changes dramatically with different flight conditions, and it was deemed that the canard was the best way to handle this as it could accommodate for these changes more easily than a tailless or conventional configuration.

The canard is designed as a 3% thick wing with a symmetric airfoil of similar characteristics to the wing. Its  $C_{L\alpha}$  is currently the same as the aircraft's delta wing. The canard itself acts as a stabilator and controls the aircraft pitch. No elevators were deemed necessary or desirable for supersonic flight conditions.

**Longitudinal Static Stability.** Longitudinal static stability was a driving factor in the vehicle's design as a statically stable aircraft equates to low cost. This is achieved through the absence of expensive stability augmentation systems (SAS) and an easily controllable aircraft. The static margin of the aircraft is one of the main criteria defining the SARRA vehicle's static stability and was calculated using a component build-up method. The neutral point was found over the entire aircraft and related to the location of the center of gravity during the mission (Etkin & Reid, 1996).

$$h_n = h_{n_{wb}} + \frac{a_t}{a} \bar{V}_H \left( 1 - \frac{\partial \varepsilon}{\partial \alpha} \right) - \frac{1}{a} \frac{\partial C_{m_p}}{\partial \alpha} + h_{n_{fus}} \quad (13)$$

Once the neutral point was obtained, it was used to find  $C_{m_\alpha}$  and  $K_n$ .

$$C_{m_\alpha} = C_{L_\alpha} (h_n - h) \quad (14)$$

$$K_n = (h_n - h) \quad (15)$$

Values, along with some justifications used in the static margin's calculation are found in Table 7. Figure 27 shows the variation of the static margin over the aircraft's mission during times when it performs maneuvers.

In order to optimize the size of the canard, a study was performed with varying canard sizes over the mission segments. The static margin range was the criteria in

**Table 7. Assorted data used in the calculations:**

$\bar{c}$	27.11 ft	$S_t$	75 ft <sup>2</sup>
$\bar{l}_t$	Varies with Mach #, ranges from 53-58 ft	$S$	1123 ft <sup>2</sup>
$\bar{V}_H$	$\frac{\bar{l}_t S_t}{\bar{c} S}$	$a$	Varies with Mach #
$\frac{\partial \varepsilon}{\partial \alpha}$	Considered negligible as canard produces very little lift and downwash	$\frac{\partial C_{m_p}}{\partial \alpha}$	Considered negligible
$h_{n_{wb}}$	Varies with Mach #, ranges from 74.5-80.3 ft (measured from nose)	$(h_{vt} - h)$	24.62 ft
$(h - h_p)$	3.65 ft		

selecting the tail size. An excessively small static margin is undesirable for the SARRA vehicle as maneuverability is not a major design concern. A large static margin is also undesirable, as stiff controls do not allow for ease of control. Figure 27 shows a range of static margins for different canard sizes. This demonstrates how the current canard was designed. An area any lower than 70 ft<sup>2</sup> (6.5 m<sup>2</sup>) would have produced an excessively large static margin, which would produce a stiff and difficult to control aircraft. A larger canard would have produced an aircraft that is almost neutrally stable at certain points, a condition that is undesirable as excessive maneuverability is not necessary for the aircraft's mission. Considering the transonic region will also have high static margins, minimizing the margin range over the course of flight is critical.

The wide variation in static margin is due to supersonic flight speeds as well as large shifting of the center of gravity. The maximum static margin that the aircraft will experience is 22.0% in the transonic region. This is not shown in Fig 27 due to the fact that maneuvers will not be taking place in the transonic region. The highest point at which the aircraft maneuvers is 13.0% at a speed of Mach 1.8.

In order to avoid a sudden change in the controllability of the aircraft, the center of gravity of the rocket is moved to a point coincident to that of the aircraft just prior to release. Fuel is also pumped to different tanks within the aircraft to ensure the proper center of gravity for a static margin of approximately 6.0%. The static margin is positive over the entire range of flight, indicating a stable aircraft.

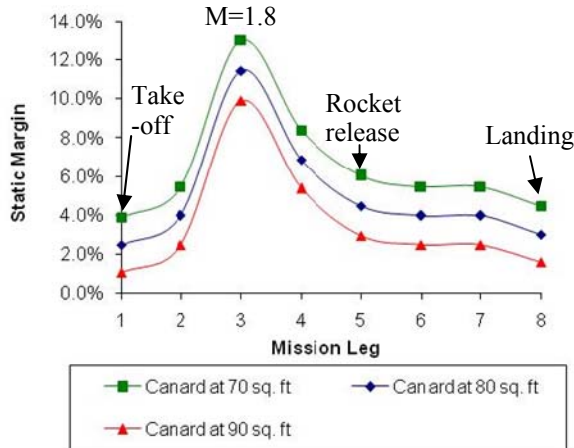


Figure 27. Sizing of the canard, Static Margin over Critical Mission Points.

Another value critical to the aircraft's longitudinal static stability is the pitching moment coefficient's derivative with respect to angle of attack ( $C_{M\alpha}$ ). In order for the aircraft to correct itself, this value must be negative during flight. The  $C_{M\alpha}$  displays trends that are directly related to those displayed by the static margin. Figure 28 shows the variation of the  $C_{M\alpha}$  over the different mission legs. Its negative trend over flight duration indicates a stable aircraft, with a small amount of pitch stiffness during take-off and landing.

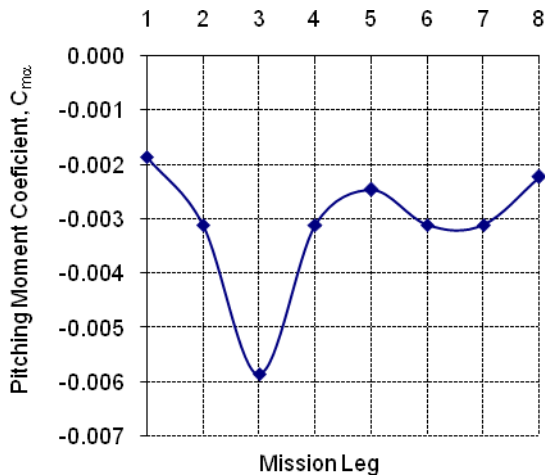


Figure 28.  $C_{M\alpha}$  over maneuverable points in the mission.

**Control Surfaces.** Control surface sizing was performed by historically analyzing the control surfaces on aircraft of similar performance qualities. By finding the area ratios of the control surfaces on the XB-70, Concorde, F-16, and other similar aircraft, an estimation of the size of the control surfaces on the SARRA vehicle was made. Refer to Table 8 for detailed information on the control surface sizes.

In place of elevators, an all-moving canard was deemed desirable. Control surface flutter is minimized at supersonic speeds, and the opportunity for more responsive longitudinal controls is present, as the entire canard, changing its angle of attack, would provide more lift than simple elevators. There are two forms of roll control present on the wing. For low speed maneuvers, ailerons are used, and high-speed maneuvers utilize inboard spoilers in order to reduce wing twist and adverse yaw effects.

Table 8. Sizing of Control Surfaces

Tail	Tail Area
$S_h$	70 ft <sup>2</sup>
$S_v$	160 ft <sup>2</sup> (each)
Control Surface	Control Surface Area
Canard	70 ft <sup>2</sup>
Ailerons (outboard)	56 ft <sup>2</sup> $\frac{s}{s_w} = .049$
Spoilers (inboard)	56 ft <sup>2</sup> $\frac{s}{s_w} = .049$

**Engine-Out Analysis.** In the event that the SARRA vehicle loses power on one side of the aircraft, it must still maintain yaw control. An engine out analysis was performed in which two engines on the same side were deemed inoperable. Vertical tails and rudders are sized in order to counteract the moment produced by the two engines still running. The analysis made use of a simplified lateral equation of motion,

$$N = F_v(h_{vt} - h) - F_p(h - h_p). \quad (16)$$

$F_v$  represents the force of the vertical tails, while  $F_p$  is the force of the propulsion system. In the case of losing two engines on the same side, the remaining engines must produce enough thrust to maintain flight. The above equation is transformed into a more useable form,

$$\frac{1}{2} \rho V^2 S_{vt} C_{L_{vt}} (h_{vt} - h) = F_p (h - h_p). \quad (17)$$

The dynamic pressure alone multiplied by area of the vertical tail produces enough force to require a small rudder deflection. According to drag numbers, the required rudder lift coefficient is 1.02 on take-off. With the rudder chord approximately 30% the size of the vertical tail chord, yaw control is maintained in the aircraft in the event that two engines go out on take-off.

**Summary of Stability and Control.** As shown from the basic analysis above, it is possible to create a SARRA vehicle that is statically stable with the ability to maintain control throughout flight. The design presented is not out of the ordinary either. Historically, this configuration has

had success with other aircraft with similar mission characteristics such as the XB-7. The stability and controls analysis above should show that this goal is not a lofty one in the stability and controls realm and is possible to achieve without the development of expensive new technologies.

### VIII. Structures

Evaluation of the stated aircraft performance requirements led to this discussion of the structural requirements and opportunities for cost savings. The mission factors, loads, load paths, critical components, materials, and manufacturing breaks for the SARRA are presented in this section.

**Mission Factors.** Structurally speaking, the most critical task and highest technical risk of the aircraft is carriage of a single 60,000 lb (27,200 kg) thin walled rocket while protecting its structural integrity and its satellite payload. The second most critical challenge faced is building a structure that allows for cost effective design, manufacturing, operation, and maintenance. Ultimately, the SARRA accomplishes both of these by supporting the rocket fully from below and remaining low cost due to simple load paths, inexpensive materials, modular manufacturing breaks, low drag geometries and durable modular structures.

Carriage of the rocket above, below, and mid way through the wing was explored. Optimum aerodynamic shapes neck down at the fuselage and wing join area, which reduces the cross sectional area and smoothes out the area distribution along the aircraft centerline, reducing drag. This simultaneously reduces the volume available to house the structure necessary to carry the central loads from the wing, rocket, and other components. The rocket could not be carried between the wings since interrupting the wing carry-through structure would produce costly drag due to routing the structure around the rocket and limiting the ability to taper the fuselage. This required the aircraft to carry more fuel in the long run and required heavy structural reinforcement in between the wings.

Reducing the drag has a larger effect on lowering GTOW than does reducing the empty weight, which in turn lowers the development and operations cost by a larger margin than reducing empty weight alone. Any carriage method that reduced drag was given precedence over the structural density at the wing-fuselage join area. The structure at the wing join is defined later. Because of higher drag penalty, the mid-carriage configuration was ruled out, which left top and bottom carriage configurations as options.

Investigating the rocket attachment and support for the two remaining configurations led to evaluating the structural implications of the rocket. The Falcon 1 is designed to withstand large accelerations in the axial

direction but not necessarily the lateral directions. It has some direct structural reinforcement to resist loads in addition to maintaining its structural rigidity with the aid of pressurized fuel and oxidizer tanks.

The rocket is attached to the aircraft at several locations along its length, and aerodynamic loading on the aircraft will transfer to the rocket. To get the most conservative estimation of deformation of the rocket structure due to these loads, attachment at hard points were assumed located only at the top and bottom of the rocket stages, and the first stage (the longest unsupported section for bottom carriage) was evaluated. Shear force, bending moment, and stress in the outer-most fiber at the midpoint of the section were calculated.

A trade study was carried out to determine the sensitivity of the largest unknown, the moment of inertia of the rocket along the y-axis. The trend showed that deflection depends greatly on the estimation of the internal structure of the rocket. This did not state conclusively that bottom carriage of the rocket is unacceptable, but it showed that more analysis must be done to determine the effects.

To reduce the amount of analysis required and the technical risk associated with bottom carriage, top carriage was chosen for the concept. This allowed support along the entire rocket length, which reduced rocket deflections and fuselage stress concentrations. In addition, this allowed the support structure on the aircraft to be designed similarly to any existing cargo floor further reducing development costs for the airframe.

**Loads.** The structure of an aircraft is necessary to maintain its shape and house the components required for flight. It resists loads encountered in the maneuvering envelope or V-n diagram, shown in Fig 29. The V-n diagram shows the maximum loading (g's as multiples of gravity) versus velocity for stall, gust, structural limit, and maximum speed for sea level, 25,000 ft (7,620 m), and 50,000 ft (15,240 m).

The maximum structural limits were chosen based upon historical precedence and the capabilities of current air-launch systems. The "Pegasus Users Guide" (Orbital, 2007) stated the maximum lateral loading that its payload sees is 3.6 g's and Raymer (1999) gave -2 g's as the typical negative loading for a tactical bomber (which is similar in flight regime and payload to the SARRA vehicle).

Historically, the -2 g load limit stems from a -3 g gust-loading while in a 1 g steady, level flight. Given the lift characteristics of the SARRA and flight regime, gust loads have very little effect on the loads that the airframe experiences. This is shown in Fig 29 by the curves marked "Gust Loading at S.L." The gust-loading plot resulted from use of Raymer's relation for gust response.

Material limits of surface heating due to shocks and friction determined the maximum velocity at 50,000 ft (15,240 m), but at sea level and 25,000 ft (7,620 m), zero excess thrust determines maximum velocity.

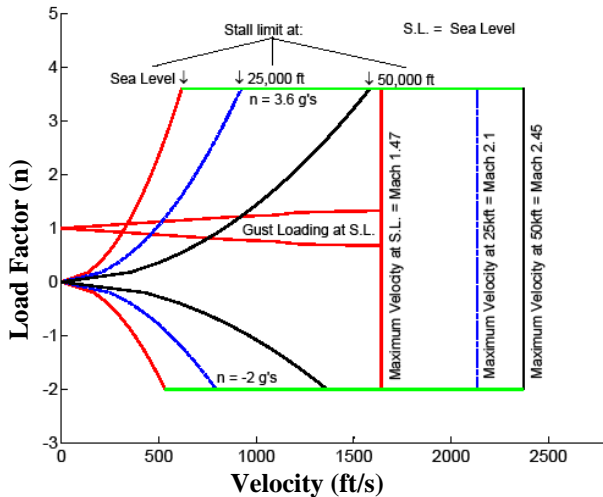


Figure 29. V-n diagram and flight envelope at sea level, 25,000 ft and 50,000 ft for the SARRA.

Limiting the carriage and launch environment loads reduced costs associated with development of this concept. The chosen maximum load conditions will limit additional research and development required for the rocket and its satellite payload by placing them in conditions already established as acceptable for air-launch methods.

Using low cost materials further reduced the cost of procurement and design of the structure. These materials provide structural integrity well into the flight regime designated for the mission, and they defined the maximum speed of the aircraft at altitudes above 30,000 ft (9,144 m). Reducing the cost by choosing materials, carriage methods, and the load environment aligned with the L-3 theme.

The discussion so far has not explained why it is important not to exceed these load factors or how they physically affect the aircraft. The general load each component experiences on the aircraft was determined by one of three broad loading cases: supersonic flight, subsonic flight, and ground loads.

These cases were characterized by the distribution of the reaction forces on the aircraft. In the supersonic case, the loads were reacted over the largest area based on lift distribution on the fuselage and wing. The subsonic case moved those reactions to only the wing spar attachments, which was still well distributed compared to the ground load case. The ground load case has the highest load concentration on the airframe, at the landing gear locations, and thus became the critical loading case.

The two graphs in Fig 30 represent the ground load. They show shear force versus centerline distance and bending moment versus centerline distance. The weight distribution was assumed uniform in 1 ft segments along the fuselage and the component weights were distributed within their geometric constraints. In these graphs, you can see the extreme shift in shear load and bending moments at the landing gear locations. As is shown, the maximum shear load also corresponds to the same location. The highest bending moment occurs midway across the expanse from the nose landing gear to the main landing gear, and the sign of the slope changes as is expected at the gear locations.

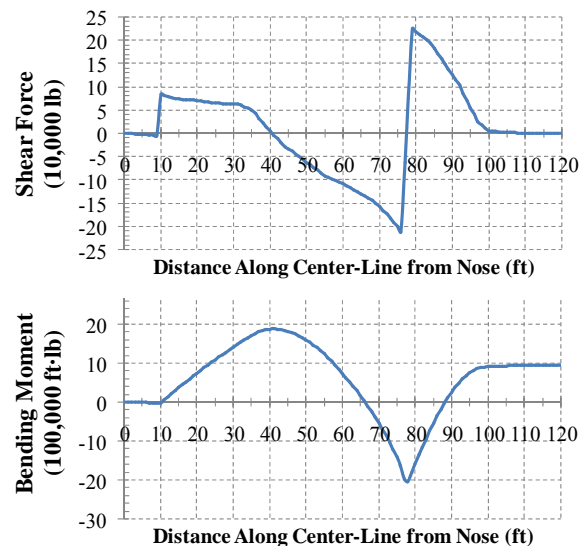


Figure 30. Shear force and bending moment diagrams for the aircraft along its centerline

In the air, the load is controlled for the most part, by how the aircraft is maneuvered. On the ground, the aircraft is subject to loads due to bumps in the pavement. Care is taken when taxiing, on liftoff, and landing so as not to exceed the loads prescribed for the payload. The aircraft was designed to the same load standards as the payload to eliminate an overly built structure.

**Load Paths.** The load factors are multiples of gravity (accelerations), which produce forces and bending in the aircraft structure as seen in Fig 30. The aircraft and everything attached to it must withstand the resulting loads and remain in usable condition. Figure 31 shows a layout of the internal structure to support these loads and their load paths.

The load passes from the landing gear to reinforced landing gear attachments on the bottom surface of the wing, which spans the load over to the centerline keelsons. In flight, the loads on the wings pass from the distributed flange wing through a solid wing box carry-through to the keelsons. The wing has shear webbing in the span and cord directions to prevent the skin flange

from buckling. The skin carries the majority of the load in the wing. The keelsons support the majority of the loads represented in Fig 30 in the fuselage. The rocket payload sits on top of the cradle (shown in Fig 32) which rests above the keelson. The keelson carries the loads forward and aft. In front of the rocket, the support members blend from a determinate load path into a more indeterminate structure. The indeterminate structural components are similar to transport aircraft with longerons, frames and stressed skin.

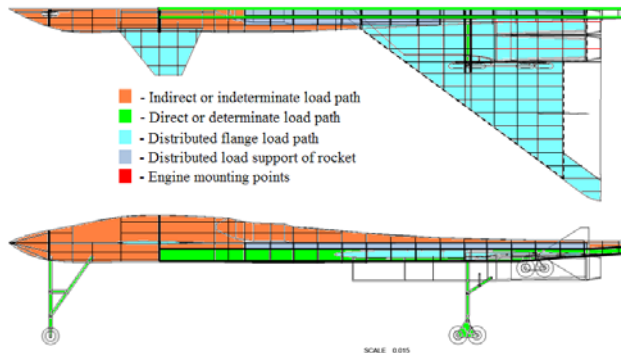


**Figure 31. Internal structure and load paths of the SARRA.**

The layout in Fig 31 simplified the load paths in the volume critical locations of the aircraft and reduced manufacturing and design costs by allowing for straight-line components and dual purpose structures (e.g. the keelson acting as the backbone for the entire aircraft and the base for the cradle).

**Rocket Cradle.** This section describes further, how the aircraft reduces the risk associated with supporting the relatively flimsy structure of the rocket. An image of the cradle that supports the rocket is shown in Fig 32. The cradle mimics a boat trailer. The skin of the rocket is analogous to the fiberglass hull of a boat in that it carries a very heavy load on a surface that is only intended to have the load fully distributed.

The cradle rails and vertical supports are themselves light weight and their only purpose is to transmit vertical and horizontal loads to the keelson. They do not need to carry any of the bending stresses in the fuselage. Each attachment point of the cradle is movable and the entire unit retracts down about 6 inches when the rocket is released. Having each attachment adjustable allows sensors to maintain an un-deformed shape in the cradle and rocket. The cradle will insulate the rocket from vibrations in the airframe and decouple bending of the rocket from bending of the fuselage.

This image shows the wing box and that the centerline vertical component of the wing box doubles as the main keelson. The secondary keelsons pass over the wing box and do not interrupt the load path. The rocket is attached to the aircraft by shackles attached to the existing hard points on the rocket. By supporting the rocket along the majority of its side and using existing hard points, less

research and development is required to clear the rocket structure for service on a vehicle of this nature. This further reduces the cost for engineering and testing.

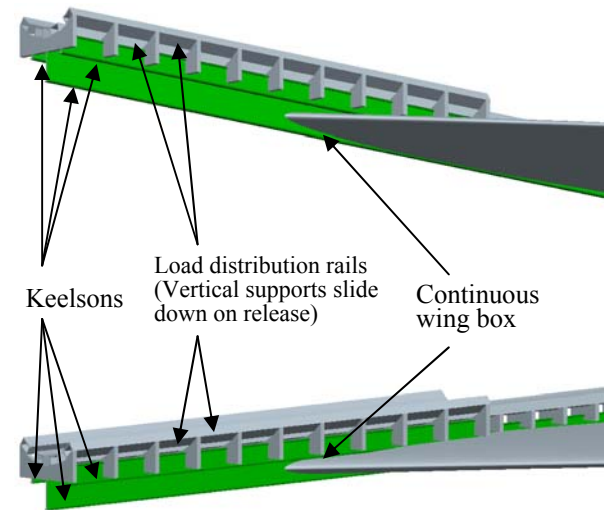


**Figure 32. Rocket cradle, keelson, and wing join detail.**

**Materials.** During discussion of the loads, it was said that the maximum velocity was set based on material limitations. In order to align material selection to the low cost theme, a decision was made to use non-exotic, inexpensive materials like cast, machined, or extruded aluminum as much as possible instead of complex, honeycomb laminates of stainless steel or titanium.

Aluminum required operating the aircraft below high velocity levels at which surface heating would degrade the integrity of the airframe. Choosing Mach 2.45 at 50,000 ft (15,240 m) limits the skin temperature range from just below 310 deg F (428 K) for non leading edge surfaces and 400 deg F (478 K) for leading edge surfaces. At these conditions, titanium is used selectively on the leading edge surfaces, but aluminum is still used widely in the substructure and non-leading edge surfaces. The effects these temperatures will have on the heat tempering of the metals are unknown, but the temperatures are low enough that if needed light coatings of heat shielding or cooling with the liquid oxygen boil off escaping from the rocket fuel tanks may mitigate all risk there.

The materials chosen are as follows:

- 4140 steel for the landing gear due to its high strength and durability and low cost, (MatWeb, 2007)
- 7075-T6 aluminum for compression skins and shear webs due to its higher strength, (MatWeb, 2007)
- 2024-T4 aluminum for tension skins due to its higher fracture toughness, (MatWeb, 2007)
- 10-2-3 titanium alloy for leading edges, engine mounts, and exhaust shielding, (MatWeb, 2007)

The different materials are selected based on the loading they experience during service. The landing gear

may carry high stress repeatedly and thus need a strong durable material. The compression skins and shear webs are much more likely to fail due to crippling or buckling and require a high compressive and shear strength alloy. The 7000 series aluminum alloys are zinc based, and they tend to have higher strength, (Howe, 2004). The tension skins are more likely to fail due to crack propagation, and a copper based aluminum alloy was chosen because they tend to have higher fracture toughness, (Howe, 2004). Finally, titanium was selected to use on the leading edges due to its well-known strength at high temperatures.

**Manufacturing Breaks.** The last area in structures with cost saving opportunities is detail design and manufacturing. The SARRA is broken down into 7 major assemblies. They are shown in Fig 33. These assemblies are the fuselage, canard, cradle, wing, engine pod, and two vertical tails. This allows detailed design, production, testing, and maintenance to occur in a modular fashion.

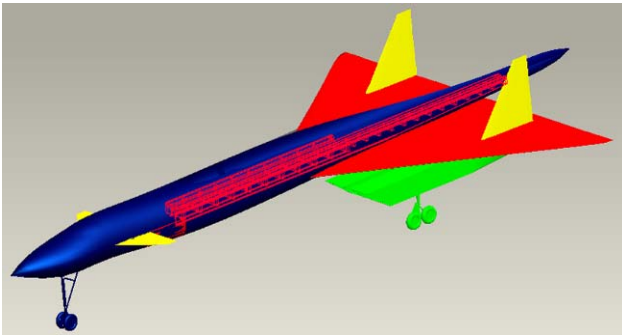


**Figure 33. Major manufacturing sub assemblies.**

The detail design of the major assemblies will take place concurrently to reduce the time required to develop each. The interfaces between each are defined by the loft lines of the aircraft and standard attachment procedures used on previous airframes. The general geometric shapes of the flanges, shear webs, and stiffeners will follow similar proven designs already in use. These both will reduce the man hours required to design the aircraft. Using established design standards will make manufacturing and testing more streamlined with predictable results. This will lower the cost of engineering, redesign, and rework on the production line.

Splitting the airframe into major assemblies gives the flexibility to outsource portions of the aircraft in order to obtain the lowest cost for the components. It also enables testing at earlier stages giving time to fix structural shortcomings independently of other parts. Once the design is decided upon, extra assemblies are produced and stored until needed later as spare parts or extra aircraft. Having the ability to produce and assemble spares will make repair less expensive.

**Summary of Structures.** Conclusions taken from structural analysis of the different concepts were that no matter what configuration the aircraft is, it must accommodate the structural limitations of the rocket and the rocket's payload. In addition, top carriage of the rocket reduces structural technical risk, weight, and development costs. Choosing a lower maximum speed, non-exotic materials, and payload based load limits all reduce the research and development and acquisition costs. Manufacturing is also considered, and cost is further reduced through splitting the major assemblies into separate products.

## IX. Cost

Cost is the most important factor in developing the SARRA vehicle. The need to lower costs in all fields is crucial to the development of a successful business model and product. Costing methods from Roskam were used (Roskam, 1987).

**Research, Production and Operation Costs.** The research and development costs are maintained at a minimum due to the use of off-the-shelf technologies. The engines were developed in the 1980's and have enjoyed extensive testing, thus making them extremely reliable. Furthermore, the flight regimen, use of non-exotic materials (steel, aluminum, and small amounts of titanium), lowering the development costs. In general, the use of known technologies allows for lower engineering trainings costs and concentrates most engineering work toward the implementation of existing technologies rather than inventing new technologies.

The cost of production for each aircraft was kept low with the use of existing materials and technology while fully integrating research and development into the manufacturing process. Redundant systems of manufacturing are not necessary for production of this aircraft. Unlike many government aircraft programs, which require redundant manufacturing lines to ensure a viable supply of war goods in the event of conflict, the SARRA vehicle does not require such practices. Combining the R&D manufacturing process with the production line simplifies the routine and allows for better synergies amongst the labor force.

The operation costs for the SARRA vehicle are low because of the utilization of known technologies, and practices. Since the SARRA vehicle is built off of existing systems, finding replacement parts is relatively simple and inexpensive. Furthermore, the use of non-exotic materials makes for easy maintenance and reduces the cost of training personnel in dealing with new materials on the aircraft. The largest component of operation is the cost of jet fuel, thus the SARRA vehicle seeks to carry the least amount of fuel possible for each mission.

Beyond the operational costs, the vehicle is expected to have low testing costs. All of the aircraft main components have been in use for many years and have been extensively tested by other companies and aircraft manufacturers.

Because replacement of the SARRA vehicle is a very costly proposition, the life span for the aircraft is set at 25 years.

**Life Cycle Cost.** With a life cycle for the SARRA vehicle of 25 years; as such, the aircraft will have the potential to make significant returns on investment. Table 9 tabulates the life cycle cost over the 25-year period for one aircraft. The cost of constructing a base of operation is included in this life cycle calculation as is the need to taken into account one-time purchases of ground equipment and other items.

**Table 9. Life cycle cost per aircraft for 3000 lifetime flights (Roskam, 1987)**

Costs	5 A/C Fleet (\$M)	2 A/C Fleet (\$M)
Acquisition (R&D & Production)	\$1,007	\$2,126
Operation	\$257	\$155
Special Construction	\$200	\$200
Ground Equipment	\$100	\$100
Life Cycle Cost	\$1,564	\$2,581

**Payload Performance Analysis.** This system reduces the total  $\Delta V$  required to place the payload carried on the Falcon 1 in orbit, from 29,200 ft/s (8900 m/s) for a vertical launch, to a  $\Delta V$  of 24,300 ft/s (7,400 m/s) for launch at Mach 2.0. The mass allocated for fuel on the Falcon 1, ordinarily used for the 29,199 ft/s (8,900 m/s) vertical launch, is now used to increase the payload mass from 1,057 lb (480 kg) for vertical launch to 2,114 lb (960 kg) for air-launch.

The cost per launch of the Falcon 1 is \$7 million for 1,057 lb, or \$6,615 per lb (\$14,583 per kg). Cost per launch is \$1.72 million for the SARRA, assuming 1,500 launches per aircraft in a production run of two over the 25-year lifespan. (In 2006, there were 200 launches of payloads ranging from 1 kg to 1000 kg (Caceres, 2005).) Assuming that the \$7 million cost also applies for air-launch, the total is \$8.72 million per launch for 2,114 lb. This system would therefore reduce the cost of launching payload to LEO from \$6,615 per lb to \$4,120 per lb (\$9,080 per kg), a 38% reduction in cost. If the market increases proportionately and five aircraft are built and fully used, the cost is \$3,800 per lb (\$8,375 per kg), representing a 43% reduction of cost. Lower launch costs could possibly be achieved at higher Mach number, although this was not investigated.

**Summary of Cost Analysis.** The SARRA vehicle is designed with cost effective performance as the main consideration. Costs have been meticulously reduced to propose the most viable business model. Through the utilization of non-exotic materials, off the shelf technology and known methods; the costs for designing, building, buying and operating the SARRA vehicle are kept to a minimum; thereby achieving the goal of cost reduction.

## X. Conclusions

With the application of the L-3 criterion throughout every step of the design process, the SARRA is able to meet all of the stated objectives with a high degree of cost savings. This vehicle designed is relatively economical and usable with a turnaround time of 48 hours. The SARRA is capable of supersonic flight above Mach 2, attaining an altitude of 50,000 ft as well as launch with an angle of inclination of 25 deg. The SARRA successfully meets and exceeds the aforementioned requirements, allowing for flexibility in potential future applications but also creating for substantial cost savings in delivering payloads into orbit.

## XI. References

- Arnaiz, Henry H., "Flight-Measured Lift and Drag Characteristics of a Large, Flexible, High Supersonic Cruise Aircraft". NASA TM X-3532, 1977.
- Burton, R., Brown, K., Jacobi, A., "Low Cost Launch of Payloads to Low Earth Orbit," AIAA Journal of Spacecraft and Rockets, Vol. 43, No. 3, May-June, 2006.
- Caceres, Marcos, "A Starting Point for Satellite Market Forecasts", Aerospace America, Reston, VA, pp. 13, 2005.
- Corke, Thomas C., Design of Aircraft, Prentice Hall Publishers, 2004.
- Hall, Charles F., "Lift, Drag, and Pitching Moment of Low-Aspect-Ratio Wings at Subsonic and Supersonic Speeds". NACA RM A53A30, 1953.
- Heitmeyer, John C., "Lift, Drag, and Pitching Moment of Low-Aspect-Ratio Wings at Subsonic and Supersonic Speeds – Plane Triangular Wing of Aspect Ratio 3 with NACA 0003-63 Section". NACA RM A51H02, 1951.
- Howe, D., Aircraft Loading and Structural Layout, AIAA, Inc., Reston, VA, pp. 379, 2004.
- Lednicer, David, "The Incomplete Guide to Airfoil Usage" located at <http://www.ae.uiuc.edu/m-selig/ads/aircraft.html>, 2006.
- MatWeb Material Property Data, "Property Search," located at <http://www.matweb.com/search/SearchProperty.asp>, 2007.
- McCormick, Barnes W., Aerodynamics, Aeronautics, and Flight Mechanics, John Wiley & Sons, New Jersey, 1995.
- Musk, Elon, "Post-Launch Summary" located at [http://kwajrockets.blogspot.com/2005\\_11\\_01\\_archive.html](http://kwajrockets.blogspot.com/2005_11_01_archive.html), 2005.

Orbital Sciences Corporation, "Fig 4-3. Pegasus Design Limit Load Factors," Pegasus User's Guide, located at <http://www.orbital.com/NewsInfo/Publications/peg-user-guide.pdf>, 2007.

Piland, Robert O., "Drag Measurements on a 1/6 Scale, Finless, Sting-Mounted NACA RM-10 Missile in Flight at Mach Numbers From 1.1 to 4.04 Showing Some Reynolds Number and Heating Effects". NACA RM L54H0, 1954.

Raymer, D.P., Aircraft Design: A Conceptual Approach, Third Edition, AIAA, Inc., Reston, VA, pp. 229-270, 379-401, 406, 408-412, 426-446, 2006.

Roskam, Jan., Airplane Design, Roskam Aviation and Engineering Corporation, Ottawa, KS, 2007.

Selig, Michael, "UIUC Airfoil Coordinates Database - Version 2.0" located at [http://www.ae.uiuc.edu/m-selig/ads/coord\\_database.html](http://www.ae.uiuc.edu/m-selig/ads/coord_database.html), 2006.

Wilcox, Floyd J., "Tangential, Semisubmerged, and Internal Store Carriage and Separation at Supersonic Speeds" AIAA Paper 91-0198, 1991.